Interaction of amisulpride with GLUT1 at the blood-brain barrier. Relevance to Alzheimer's disease

Sevda T. Boyanova[1], Ethlyn Lloyd-Morris[1], Christopher Corpe[2], K. Miraz Rahman[1], Doaa B. Farag[3], Lee K. Page[1], Hao Wang[1], Alice L. Fleckney[1], Ariana Gatt[4], Claire Troakes[5], Gema Vizcay-Barrena[6], Roland Fleck[6], Suzanne J. Reeves[7], and Sarah A. Thomas[1 *]

[1] King's College London, Institute of Pharmaceutical Science, 150 Stamford St, SE1 9NH, London, UK; [2] King's College London, Department of Nutritional Sciences, School of Life Course Sciences, Faculty of Life Sciences and Medicine, [3]Faculty of Pharmacy, Misr International University, 11431, Cairo, Egypt; [4] King's College London, Wolfson Centre for Age Related Disease, 20 Newcomen St, SE1 1YR, London, UK; [5] King's College London, London Neurodegenerative Diseases Brain Bank, IoPPN, De Crespigny Park, SE5 8AF, London, UK; [6] King's College London, Centre for Ultrastructural Imaging, New Hunt's House, Guy's Campus, SE1 1UL, London, UK; [7]Faculty of Brain Sciences, University College London, 149 Tottenham Court Road, W1T 7NF, London, UK

Running title or short title: Interaction of amisulpride with GLUT1 at the blood-brain barrier.

[*]Correspondence:

sarah.thomas@kcl.ac.uk[1] King's College London, Institute of Pharmaceutical Science, 150 Stamford St, London SE1 9NH, UK

Abstract

Blood-brain barrier (BBB) dysfunction may be involved in the increased sensitivity of Alzheimer's disease (AD) patients to antipsychotics, including amisulpride. Studies indicate that antipsychotics interact with facilitated glucose transporters (GLUT), including GLUT1, and that GLUT1 BBB expression decreases in AD. We tested the hypotheses that amisulpride (charge: +1) interacts with GLUT1, and that BBB transport of amisulpride is compromised in AD.

GLUT1 substrates and inhibitors, and GLUT-interacting antipsychotics were identified by literature review and their physicochemical characteristics summarised. Interactions between amisulpride, and GLUT1 were studied using *in silico* approaches and the human cerebral endothelial cell line, hCMEC/D3. Brain distribution of [^{3}H]amisulpride was determined using *in situ* perfusion in wild type (WT) and 5xFamilial AD (5xFAD) mice. With transmission electron microscopy (TEM) we investigated brain capillary degeneration in WT and 5xFAD mice, and human samples. Western blots determined BBB transporter expression in mouse and human.

Literature review revealed that, although D-glucose has no charge, charged molecules can interact with GLUT1. GLUT1 substrates are smaller (184.95±6.45g/mol) than inhibitors (325.50±14.40g/mol), and GLUT-interacting antipsychotics (369.38±16.04). Molecular docking showed beta-D-glucose (free energy binding: -15.39kcal/mol) and amisulpride (-29.04kcal/mol) interact with GLUT1. Amisulpride did not affect [^{14}C]D-glucose accumulation in hCMEC/D3. 5xFAD mice showed increased brain [^{3}H]amisulpride uptake, and no cerebrovascular space changes compared to WT. TEM revealed brain capillary degeneration in human AD. There was no significant effect of

AD on mouse GLUT1 and P-gp BBB expression, and in human GLUT1 expression. In contrast, caudate P-glycoprotein expression was decreased in human AD capillaries versus controls.

This study provides new details about the BBB transport of amisulpride, evidence that amisulpride interacts with GLUT1, and that BBB transporter expression is altered in AD. This suggests that antipsychotics exacerbate the cerebral hypometabolism in AD. Further research into the mechanism of amisulpride transport by GLUT1 is important for improving antipsychotics safety.

Keywords: blood-brain barrier; amisulpride; adverse events; transporters; GLUT1.

66 # Introduction

67 Psychosis, which most commonly presents as delusions, is highly prevalent (~50%) in
68 people with Alzheimer's disease (AD) (1,2), and is associated with poorer quality of life,
69 a more rapid speed of cognitive and functional decline (2) and greater risk of
70 institutionalisation (3). Safe and effective prescribing of antipsychotic drugs is
71 challenging in older people, particularly those with AD, due to their heightened
72 susceptibility to the side effects of these drugs (4), including sedation, postural
73 hypotension, parkinsonism, and an increased risk of stroke and death (5,6). As a result,
74 antipsychotic use is restricted to those with severe psychosis and/or aggression that have
75 not responded to non-pharmacological approaches. In the UK, the National Institute for
76 Health and Care Excellence guidance advocates use of 'the lowest possible dose for the
77 shortest possible time' (7). There is a lack of guidance on the minimum clinically
78 effective dose for individual drugs, or the factors that predict differing response and side
79 effects, although a recent publication, based on clinical data on risperidone use in AD,
80 suggests that increased dementia severity is an independent risk factor for emergent
81 parkinsonism (7).
82
83 Amisulpride is a second-generation antipsychotic – a substituted benzamide derivative,
84 which is a highly selective dopamine D2 receptor antagonist (8). It can be prescribed off-
85 label in very late onset (> 60 years) schizophrenia-like psychosis (9), and in patients with
86 AD psychosis (10–12). Therapeutic drug monitoring studies in adults predominantly
87 aged under 65 years have shown that therapeutic striatal D2/3 receptor occupancies
88 between 40-70% are achieved at blood drug concentrations of 100-319 ng/ml; equivalent

89 to 400-800 mg/day (13–15). Older patients with AD psychosis (aged 69-92 years)
90 showed a clinical response to amisulpride and parkinsonian side effects at lower doses
91 (25-75 mg/day) with high D2/3 receptor occupancies in the caudate (41-83%) and lower
92 blood drug concentrations (40-100 ng/ml) than expected (11,12).
93
94 These findings suggest that age and/or AD-related changes in central pharmacokinetics
95 contribute to antipsychotic drug sensitivity and implicate the blood-brain barrier (BBB)
96 which controls the entry of drugs to the brain through selective transport pathways.
97 Evidence from our animal studies further supports this hypothesis (16). Since
98 amisulpride is predominantly positively (17) charged at physiological pH, observed
99 changes in the expression and/or function of BBB transporters for organic cations may
100 help explain the increased amisulpride sensitivity in AD patients. In particular, the
101 organic cation transporter 1 (OCT1; SLC22A1) and the plasma membrane monoamine
102 transporter (PMAT; SLC29A4) (16).
103
104 Compromised function and expression of other SLC transporters at the BBB, such as the
105 glucose transporter, GLUT1 (SLC2A1), has also been observed in AD (18–20).
106 Consequently, AD brains suffer chronic shortages of energy-rich metabolites (21,22).
107 Importantly, antipsychotic drugs, including risperidone and clozapine, inhibit glucose
108 uptake by transporters, it has been suggested that this could be through direct interaction
109 with GLUT transporters (23,24). In addition, the use of clozapine and another
110 antipsychotic drug, olanzapine, has been associated with the development of type 2
111 diabetes. One of the proposed mechanisms is through the inhibition of glucose
112 transporters inducing hyperglycaemia (25–27). However, detailed studies of the drugs-

113 transporter interaction, including *in silico* molecular docking studies on the specific
114 molecular interactions of antipsychotics with GLUT1 are rare.
115
116 Thus, considering the changes in GLUT1 expression at the BBB and resulting impact on
117 brain metabolism in AD, and the increased sensitivity of AD patients to antipsychotic
118 drugs including risperidone and amisulpride, we wanted to explore the interaction
119 between GLUT1 and amisulpride. To do this we tested the hypotheses that amisulpride
120 interacts with GLUT1 at the BBB, and that expression of BBB transporters and the
121 transport of amisulpride and glucose into the brain will be affected by AD. We utilised a
122 combination of literature review, physicochemical properties analysis, molecular
123 docking approaches, cell culture BBB studies, studies in wild type mice and in an animal
124 model of AD and assessment of tissue from human cases with and without AD. An
125 overview of the methods deployed are presented in Supplementary Fig 1, S1 File.
126 Abstracts of this work have been presented (28).
127

128 Materials and Methods

129 Radiolabelled and non-labelled chemicals

130 Radiolabelled [^{14}C]D-glucose (#NEC042X050UC, Lot: 2389266, specific activity 275
131 mCi/ mmol) and [^{3}H]mannitol (#NET101001MC, Lot: 3632303, specific activity 12.3
132 Ci/ mmol) were purchased from Perkin Elmer. [O-methyl-^{3}H]amisulpride (MW 374.8
133 g/mol; specific activity 77 Ci/mmol; 97% radiochemical purity) was custom tritiated
134 (#TRQ41291 Quotient, UK). [^{14}C(U)]Sucrose (MW 359.48 g/mol; specific activity 536
135 mCi/mmol; 99% radiochemical purity: # MC266) was purchased from Moravek

136 Biochemicals, USA. Non-labelled amisulpride (MW 369.5 g/mol, > 98% purity) was
137 purchased from Cayman Chemicals, UK (#71675-85-9), and non-labelled D-glucose
138 (#10117) was purchased from BDH.
139

140 Literature review

141 Three different groups of molecules, which interacted with GLUT, were identified by
142 literature review. These groups were GLUT1 substrates, GLUT1 inhibitors and GLUT-
143 interacting antipsychotics. The inclusion criteria are explained below.
144

145 Identification of GLUT1 substrates and inhibitors

146 To identify established substrates and inhibitors of GLUT1 we performed a Pubmed
147 literature search using the parameters ((GLUT1 substrate) OR (GLUT1 inhibitor)) AND
148 (review [Publication Type])) AND (("1985" [Date - Publication]:"2021" [Date -
149 Publication])) (29) and tabulated the results. In the substrates group we included
150 molecules for which there is *in vitro* evidence that they are transported by GLUT1 and
151 that their uptake into cells is inhibited by established GLUT1 inhibitors, such as
152 cytochalasin B. In the inhibitors group we included molecules that were shown to
153 decrease uptake of GLUT1 substrates *in vitro*, and for which there is a proposed
154 inhibitory mechanism of interaction with GLUT1.
155

156 Identification of antipsychotics that interact with GLUT

157 We also performed a Pubmed search to identify antipsychotics which interacted with
158 GLUT transporters, using the parameters (((GLUT) AND (antipsychotic)) AND

159 (("1985"[Date - Publication]: "2021"[Date - Publication])) (accessed 04/03/2022). In the
160 antipsychotics group we included both typical and atypical antipsychotics that decreased
161 the uptake of GLUT1 substrates *in vitro*.
162

163 Physicochemical characterisation of GLUT1 substrates and inhibitors, 164 and GLUT-interacting antipsychotics

165 The physicochemical characteristics of each member of the three groups (i.e. GLUT1
166 substrates, GLUT1 inhibitors and GLUT-interacting antipsychotics) was obtained from
167 the chemical property databases, DrugBank (30) or MarvinSketch (version 22.9.0, 2022,
168 ChemAxon) (31) and tabulated.
169
170 Specifically, information about the structure and molecular weight (MW) was obtained
171 from the DrugBank (30). The mean MW ± SEM, and the median MW of the three groups
172 was then calculated and the results compared.
173
174 The gross charge distribution at pH 7.4 of each molecule was then obtained from
175 MarvinSketch. The mean gross charge distribution at physiological pH (± SEM) of the
176 three groups was then calculated and the results compared. The number of microspecies
177 of each molecule at pH7.4 was examined and the percentage prevalence and charge of
178 the top two microspecies was then reported (MarvinSketch). The physicochemical
179 characteristics of the three groups were compared to those obtained for amisulpride.
180

181 ## *In silico* molecular docking

182 *In silico* molecular docking was used to examine the molecular level interactions of
183 amisulpride, alpha-D-glucose, beta-D-glucose, and sucrose with GLUT1 using the
184 molecular docking tool GOLD. The main endogenous substrate of GLUT1 is D-glucose,
185 which is a monosaccharide present in the body as anomers: 36% alpha-D-glucose and
186 64% beta-D-glucose (32). In this molecular docking study alpha-D-glucose and beta-D-
187 glucose were used as positive controls. Sucrose is a plant disaccharide which is thought
188 not to interact with GLUT1 and was used as the negative control.
189
190 The GLUT1 Protein Database (PDB) code used was 5EQI – the crystal structure of
191 human GLUT1. The 5EQI crystal structure is for the inward open conformation of the
192 transporter which has been reported to be the most favourable for ligand binding (33).
193
194 The results from the molecular docking simulations were expressed as a free energy
195 binding and chem score. A molecule is considered a substrate for a given transporter if
196 their interaction has a free energy binding of ≤5kcal/mol and has a high chem score. The
197 chem score is one of the scoring functions of the molecular docking program. It provides
198 information on the strength of the interaction between ligand and binding sites.
199

200 ## *In vitro* studies in model of the human BBB (hCMEC/D3 cells)

201 The human cerebral microvessel endothelial cells/D3 (hCMEC/D3) are an immortalised
202 human adult brain endothelial cell line. This is a well-established and characterised
203 model, regularly used to study the human BBB (16,34). The hCMEC/D3 cell line

204 originated from human brain tissue obtained following surgical excision of an area from
205 the temporal lobe of an adult female with epilepsy (34).
206 hCMEC/D3 cells were used to study the interaction between GLUT1 and amisulpride.
207 To do this, the expression of a functional GLUT1 was first confirmed using Western blot
208 (WB) and accumulation assays with [^{14}C]D-glucose. This was followed by further
209 accumulation assays with [^{14}C]D-glucose and non-labelled amisulpride. [^{3}H]mannitol
210 was used as a marker of cellular integrity and non-specific binding to the membranes
211 and plastic wear. The hCMEC/D3 cells (passages 30-35) were grown as described
212 previously by Sekhar et al., 2019 (16). All experiments were carried out at King's
213 College London, in accordance with the guidelines of the Local Ethics Committee and
214 research governance guidelines.
215

216 Western blot studies – expression of GLUT1 in hCMEC/D3 cells

217 Cells were grown for four to five days in T-75 flasks until they formed a fully confluent
218 monolayer, and then for another two to three days before harvesting and preparing lysates
219 for WB. Lysates were prepared by placing the flask on ice, aspirating the medium and
220 washing the cells in ice-cold phosphate buffered saline (#70011-36 Gibco, Fischer
221 Scientific Ltd, UK). The cells were then incubated on a shaker for 10 minutes in radio-
222 immunoprecipitation assay (RIPA) buffer (#R0278, Sigma, UK) and 1% (v/v) protease
223 inhibitors (#78441, Thermo Fisher Scientific, UK) for cell lysis and protein
224 solubilisation. The cells were then scraped off from the bottom of the flask and
225 transferred to an Eppendorf tube. The tube was then agitated for 20 to 30 minutes at 4°C.
226 Next, the cell suspension was centrifuged (Biofuge Fresco, Heraeus Instruments, UK)

227 for 20 minutes at 11,753 x G at 4°C. The resulting supernatant (protein lysate) was snap
228 frozen in liquid nitrogen. Before the start of the WB procedure, the protein lysates were
229 thawed and the total protein concentration in each lysate was estimated by bicinchoninic
230 acid (BCA) assay using bovine serum albumin standards (Thermo Scientific, UK) as
231 described by Sekhar et al., 2019 (16).
232
233 The protein lysates for WB were mixed with sample loading buffer (1:4) (#NP0007
234 NuPAGE LDS Sample Buffer (4x), Invitrogen, Carlsbad, USA), reducing agent (1:10)
235 (#B0009, Novex by Life Technologies, USA), and RIPA buffer. Once prepared, they
236 were heated at 95°C for 5 minutes. The rest of the WB procedure was performed as
237 described in (16) except, 30 µg of protein was loaded in each well, antibody solutions
238 were made in 5% milk in TBS-T, and washes were performed in TBS-T (for antibodies
239 dilutions see Supplementary Table 1, S1 File). Quantification of protein expression was
240 determined by calculating the intensity ratio of the band of interest and the band of the
241 loading control (GAPDH). Band intensity ratio analysis was conducted using ImageJ
242 software (35).
243

244 Accumulation assays – function of GLUT1 in hCMEC/D3 cells

245 The cell culture method and experimental design of the accumulation studies are
246 described in the following sections. The cells were grown as already described in the "*In*
247 *vitro* studies" section. They were split at 80-90% confluence and were seeded at 25,000
248 cells/cm^2 in the central 60 wells of 96 well plates for accumulation assay experiments
249 (#10212811, Fisher Scientific, UK). They were grown for four to five days until they

250 formed a fully confluent monolayer, and then for another two to three days before the
251 start of the accumulation assay.

252 For the control accumulation assay experiments, the hCMEC/D3 cells were incubated in
253 an accumulation buffer (135 mM NaCl, 10 mM HEPES, 5.4 mM KCl, 1.5 mM
254 $CaCl_2H_2O$, 1.2 mM $MgCl_2.H_2O$, 1.1 mM D-glucose - the standard non-labelled D-
255 glucose concentration for the accumulation buffer, and water, pH = 7.4) for 1 h. The
256 buffer also contained [^{14}C]D-glucose (3 μM) and [^{3}H]mannitol (0.05 μM). [^{3}H]Mannitol
257 was used as a marker for non-specific binding, and barrier integrity (36,37). All treatment
258 conditions contained 0.05% DMSO. Incubation was performed in a shaker at 37°C and
259 120 rotations per minute. Next, the cells were washed with ice-cold phosphate buffered
260 saline (#BR0014G, Oxoid Limited, England) to stop the accumulation process and to
261 remove any radiolabelled molecules and buffer that had not entered the cells. Then the
262 cells were incubated in 1% Triton X (200 μl per well) for 1 h at 37°C, to solubilise the
263 cell membranes, and to free any accumulated radiolabelled compounds via lysis. Half of
264 the cell Triton X lysate from each well was pipetted into a scintillation vial and 4 ml of
265 scintillation fluid (#6013329, Ultima GoldTM, Perkin Elmer, USA) was added. The
266 amount of ^{14}C and ^{3}H radioactivity in the sample was measured in disintegrations per
267 minute (dpm) on a Tricarb 2900TR liquid scintillation counter. The dpm of each sample
268 were corrected for background dpm. The background dpm was determined from a vial
269 containing 100 μl 1% Triton X and 4 ml liquid scintillation fluid only. The remaining
270 cell lysate in the plate was used for total protein concentration control in each well,
271 determined by BCA analysis (17).
272

273 In our self-inhibition studies, investigating the presence of a functional GLUT1
274 transporter in the hCMEC/D3 cells, the cells were incubated with accumulation buffer,
275 containing [^{14}C]D-glucose (3 μM), [^{3}H]mannitol (0.05 μM) and 4 mM non-labelled D-
276 glucose. The 4 mM total concentration of non-labelled D-glucose included the standard
277 1.1mM non-labelled D-glucose normally present in accumulation buffer. Radioactivity
278 uptake was compared to the control condition in which the cells were treated with
279 accumulation buffer of the same composition apart from the non-labelled D-glucose
280 content which was 1.1 mM (the standard non-labelled D-glucose concentration in the
281 accumulation buffer). All treatments contained 0.05% DMSO. After 1 h incubation, the
282 cells were lysed and used for liquid scintillation counting and BCA assay as already
283 described. The non-labelled D-glucose concentration for the treatment condition (4 mM)
284 was selected based on previous reports that normal plasma glucose concentrations are
285 kept in a narrow range between 4 and 8 mM in healthy subjects (38) and on preliminary
286 experiments studying the effect of 4, 6, and 9 mM non-labelled D-glucose on the
287 membrane integrity of hCMEC/D3 cells (see Supplementary Fig 2, S1 File).

288 In order to assess the effect of amisulpride on the transport of D-glucose through the
289 hCMEC/D3 membrane, non-labelled amisulpride (20, 50, or 100 μM) was added to the
290 accumulation buffer, containing [^{14}C]D-glucose (3 μM), [^{3}H]mannitol (0.05 μM), and
291 non-labelled D-glucose (1.1 mM - total standard concentration of non-labelled D-glucose
292 in the accumulation buffer). All treatment conditions contained 0.05% of DMSO. The
293 cells were incubated with this mixture for 1 h, the BCA assay and liquid scintillation
294 counting was performed as described previously.

295 The total cellular accumulation of [^{14}C]D-glucose was expressed as a volume of
296 distribution (V_d; µl/mg). V_d was calculated as the ratio of disintegrations per minute
297 (dpm)/mg protein in the Triton X lysate to dpm/ µl of the accumulation buffer. The V_d
298 values for [^{3}H]mannitol were subtracted from the V_d values for [^{14}C]D-glucose to correct
299 for cell membrane integrity. This value was then divided by the protein content in each
300 well to correct for protein content. Values were expressed as a mean ± SEM.
301
302 Statistical analysis of the results from the self-inhibition studies was performed using
303 unpaired one-tailed Student's t-test. The results from the studies of the interaction
304 between amisulpride and GLUT1 were analysed using One-way ANOVA. All statistical
305 analysis was performed with GraphPad Prism 9.0.

306 Animal model studies in WT and 5xFamilial AD (FAD) mice

307 The 5xFAD mice are a model of AD which carry human amyloid-β precursor
308 protein (APP) with the Swedish (K670N, M671L), Florida (I716V), and London (V717I)
309 FAD mutations along with human PSEN-1 with two FAD mutations: M146L and L286V
310 under the murine Thy-1 promotor (39). This model has been described as one of the few
311 models that shows several AD hallmarks, including neural loss, neurodegeneration,
312 gliosis, and spatial memory deficits (40).
313
314 We confirmed the model phenotype in the following ways: comparing the weight of
315 females and males from the two genotypes; using transmission electron microscopy
316 (TEM) to confirm the presence of amyloid plaques in the brain of 5xFAD mice;
317 comparing the expression of APP in brain capillary enriched pellets isolated from WT

318 and 5xFAD mice. Enrichment of the pellets with brain endothelial cells was confirmed
319 using transferrin receptor 1 (TfR1) as an endothelial cell marker.
320

321 Animal husbandry

322 All *in vivo* experiments were performed in accordance with the Animal Scientific
323 Procedures Act (1986) and Amendment Regulations 2012 and with consideration to the
324 Animal Research: Reporting of *In Vivo* Experiments (ARRIVE) guidelines. The study
325 was approved by the King's College London Animal Welfare and Ethical Review Body.
326 The UK government home office project license number was 70/7755.
327

328 The mice were housed at King's College London in groups of three or four under
329 standard conditions (20-22°C, 12 h light/dark cycle) with food and water *ad libitum*.
330 They were housed in guideline compliant cages. Animal welfare was assessed daily by
331 animal care technicians. Animals were identified by earmarks. The experimenter was not
332 blinded to the mouse genotype.
333

334 The WT (C57/BL6) mice and the 5xFAD mice (on C57/BL6 background) were between
335 4.5 and 15 months old. The average lifespan of the C57/BL6 mice has been reported to
336 be 30 months (41). Whereas the 5xFAD mice have been reported to have lifespan of
337 approximately 15 months (42), with some authors reporting a median lifespan of up to
338 24.6 months (41).
339

340 **TEM ultrastructural study**

341 To assess Aβ plaque presence in the brain in WT and 5xFAD mice we used TEM. All
342 studied animals were female. The animals of each genotype were grouped into two age
343 ranges. The groups were WT 4.5-6 months, 5xFAD 6 months, WT 12 months, 5xFAD
344 12 months with n=2 mice per group. The weight of the animals was between 21.9 g and
345 26.7 g. For brain dissection, all animals were terminally anaesthetised with
346 intraperitoneal injection of pentobarbital (100 µl/animal) (Fort Dodge, Southampton,
347 UK).
348
349 Once each mouse was anaesthetised, it was perfuse-fixed. The left ventricle of the heart
350 was infused with ice-cold phosphate buffered saline and the right atrium sectioned to
351 provide an open circuit. Once the vasculature was free of blood, 4% paraformaldehyde
352 (PFA, #F017/2, TAAB, UK) was infused via the heart. Fixation with 4% PFA was
353 performed for 10 minutes. The brain was then removed, and the frontal cortex was
354 dissected, and cut into 1 mm^3 samples.

355 The brain samples were processed, and sectioned for TEM, and then imaged. The
356 samples were incubated overnight at 4°C in TEM fixative, containing 2.5% (v/v)
357 glutaraldehyde in 0.1 M cacodylate buffer (pH 7.3). The tissues were post fixed in 1%
358 (w/v) osmium tetroxide (#O021, TAAB, UK) for 1.5 h at 4°C. Then they were washed
359 and dehydrated through serial graded incubations in ethanol: 10%, followed by 70%, and
360 100%. The tissue was infiltrated in embedding resin medium (#T028, TAAB, UK) for 4
361 h at room temperature. The samples were embedded on flat moulds and polymerised at
362 70°C for 24 h. Ultrathin sections (100-120 nm) were cut on a Leica ultramicrotome

363 (Leica microsystems, Germany) and mounted on mesh copper grids. They were
364 contrasted with uranyl acetate for 2 minutes and with lead citrate for 1 minute. The
365 sections were imaged on an EM-1400 (Plus) transmission microscope operated at 120
366 kV (JEOL USA, Inc.).
367
368 For each frontal cortex sample, a minimum of three images were collected, and amyloid
369 plaques were identified and labelled with reference to electron microscopic atlas of cells,
370 tissues, and organs (43). The dimensions of each image were 3296x2472 pixels.

371 Western blot studies

372 We isolated the brain capillaries of each mouse used in the *in situ* brain perfusion
373 experiments. The mouse brain was *in situ* perfused via the heart with artificial plasma,
374 infused with rabiolabelled amisulpride and radiolabelled sucrose for 10 minutes. Then it
375 was homogenised in capillary depletion buffer (10.9 mM HEPES, 141 mM NaCl, 4 mM
376 KCl, 2.8 mM $CaCl_2$ (aqueous solution - 1M), 1 mM $MgSO_4.7H_2O$, 1 mM NaH_2PO_4, 10
377 mM glucose) (brain weight x 3) and 26% dextran (MW 504.4 g/mol) (#J14495.A1,
378 VWR, UK) (brain weight x 4). The homogenate was centrifuged at 5,400 G for 15 min
379 at 4°C. This resulted in separation of an endothelial cell-enriched pellet and a supernatant
380 containing the brain parenchyma and interstitial fluid. Half of the capillary pellets were
381 snap frozen in liquid nitrogen and used for WB analysis to test for TfR1, and BBB
382 transporter expression, including GLUT1, and P-glycoprotein (P-gp).
383
384 For WB, the mouse endothelial cell enriched capillary pellets were thawed, homogenised
385 in 250 µl RIPA buffer with added protease inhibitor (1% v/v). The tissue was incubated

386 in the buffer at 4°C for 30 minutes and then centrifuged (Biofuge Fresco, Heraeus
387 Instruments, UK) at 7,999 G for 15 minutes at 4°C. The resulting supernatant was used
388 for WB analysis. The rest of the WB procedure was performed as previously described
389 in this paper. For antibodies used, see Supplementary Table 1, S1 File.
390 Quantification of protein expression was determined by calculating the intensity ratio of
391 the band of interest and the band of the loading control (GAPDH or tubulin). Band
392 intensity ratio analysis was conducted using ImageJ software (35).
393
394 Unpaired two-tailed Student's t-test was used for statistical analysis of the difference in
395 expression of each transporter studied between the WT and the 5xFAD mice.
396

397 ## *In situ* brain perfusions

398 The *in situ* brain perfusion technique allows examination of the movement of slowly
399 moving molecule across the BBB in the absence of systemic metabolism. This method
400 was used to compare [^{3}H]amisulpride and [^{14}C]sucrose uptake into the brain in WT and
401 in 5xFAD mice.
402
403 The mice were terminally anaesthetised with medetomidine hydrochloride (2 mg/kg,
404 Vetoquinol UK Limited) and ketamine (150 mg/kg, Pfizer, UK, and Chanelle, UK),
405 injected intraperitoneally. Heparin was injected intraperitoneally before the perfusion
406 (100 units heparin dissolved in 0.9 % NaCl (aqueous solution) (heparin – batch number:
407 PS40057; NaCl - Sigma Aldrich, Denmark). Two experimental groups were perfused –
408 WT (12-15 months old, n=7, n=4 females, n=3 males) and 5xFAD (12-15 months old,

409 n=7, n=4 males, n=3 females). Weights of the perfused mice were between 16.8 g and
410 41.5 g. Animals with a weight lower than 25 g were excluded from the perfusion analysis
411 as perfusion at a flow rate of 5.5 ml/min could cause loss of BBB integrity (44) but their
412 capillary lysates were used in WB experiments.

413 Artificial plasma was used in the perfusion experiments. It contained 117 mM NaCl, 4.7
414 mM KCl, 2.46 mM $MgSO_4.7H_2O$, 24.8 mM $NaHCO_3$, 1.2 mM KH_2PO_4, 2.5 mM $CaCl_2$
415 (aqueous solution - 1M), 39 g/L Dextran, 10 mM glucose, 1g/L bovine serum albumin,
416 and it was mixed with Evan's blue dye (0.0551 g per 1 L of artificial plasma, #E2129-
417 10G, Sigma Life Science, India). It was warmed to 37°C and oxygenated by 95%
418 O_2/5%CO_2 gas bubbled through the solution. The artificial plasma also contained
419 [^{3}H]amisulpride (6.5 nM) and [^{14}C]sucrose (9.4 μM). Perfusion time was 10 minutes.

420 After the perfusion, the brain was dissected out and weighed. The frontal cortex, striatum,
421 thalamus, and hypothalamus were dissected under a microscope (Leica, Wetzlar,
422 Germany), weighed, and solubilised in Solvable (#6NE9100, PerkinElmer, Inc., USA)
423 for 2-3 days, then they were taken for liquid scintillation counting. These regions were
424 selected to compare with data from other *in situ* brain perfusion experiments and
425 observations from human brain data sets (16) focused on similar areas, including the
426 caudate nucleus and the putamen which are part of the striatum (45).

427 The rest of the brain was used for capillary depletion as already described. The whole
428 brain homogenate, supernatant (containing brain parenchyma and interstitial fluid), and
429 half of the capillary pellets were also solubilised and used for liquid scintillation
430 counting.

431 The concentration of [^{3}H] or [^{14}C] radioactivity present in the brain (disintegrations per
432 minute per gram of tissue – dpm/g) was expressed as a percentage of the concentration
433 of radioactivity detected in the artificial plasma (disintegration per minute per millilitre).
434 The value obtained was named %Uptake showing the radioactivity in ml/g of tissue x
435 100. The %Uptake values for [^{3}H]amisulpride were corrected for vascular space by
436 subtracting the corresponding [^{14}C]sucrose Uptake values from the [^{3}H]amisulpride
437 Uptake values.

438 Statistical analysis of the difference between the uptake of [^{14}C]sucrose corrected
439 [^{3}H]amisulpride into the brain of WT and 5xFAD was performed using unpaired two-
440 tailed Student's t-test for the capillary pellet, supernatant, and homogenate . The
441 difference between WT and 5xFAD mice in the [^{3}H]amisulpride uptake in the brain areas
442 studied was analysed with Mixed-effects analysis with Holm-Sidak post hoc test. The
443 same tests were used to analyse the difference in the [^{14}C]sucrose brain uptake between
444 WT and 5xFAD mice.

445 Human control and AD tissue studies

446 We used TEM to examine the brain and brain capillary ultrastructure of an AD case.
447 Brain capillary depletion samples from age-matched human control and AD cases were
448 used to evaluate and compare the total protein levels and the expression levels of TfR1,
449 GLUT1 and P-gp in the two groups.
450

451 Ethics statement

452 Human tissue brain samples were provided via Brains for Dementia Research (BDR) and
453 were anonymised. Written consent was provided by BDR and the specific BDR reference
454 numbers were: TRID_170, TRID_170 amendment, TRID_265 and TRID_287.
455 BDR has ethical approval granted by the National Health Service (NHS) health research
456 authority (NRES Committee London-City & East, UK: REC reference:08/H0704/128+5.
457 IRAS project ID:120436). Tissue samples were supplied by The Manchester Brain Bank
458 and the London Neurodegenerative Diseases Brain Bank, both of which are part of the
459 BDR programme, jointly funded by Alzheimer's Research UK and Alzheimer's Society.
460 Tissue was received on the basis that it will be handled, stored, used, and disposed of
461 within the terms of the Human Tissue Act 2004. The human samples were collected
462 during February 2012 to February 2019. The human tissue studies were conducted during
463 1st October 2018 to 29th January 2021. The authors conducting the human tissue analysis
464 studies did not have access to information that could reveal the identity of the human
465 tissue donors.
466

467 **TEM ultrastructural study**

468 The tissue used was from one case which was received from the London
469 Neurodegenerative Diseases Brain Bank, Denmark Hill, King's College London. Case
470 details: BBN002.32856; sex: female; age: 74; post-mortem delay: 19 h; pathological
471 diagnosis: Alzheimer's disease, modified Braak staging (BrainNet Europe – BNE
472 staging) stage VI.
473

474 Samples with size of up to 1 x 5 x 1 mm were dissected from the frontal cortex, caudate
475 and putamen. Each sample was immersed in TEM fixative (2.5% glutaraldehyde in 0.1M
476 cacodylate buffer) and incubated overnight at 4°C. The samples were then post-fixed in
477 1% (w/v) osmium tetroxide (#O021, TAAB, UK) for 1.5 h at 4°C. Then they were
478 washed and dehydrated through serial graded incubations in ethanol - 10% ethanol,
479 followed by 70%, followed by 100%. The tissue was infiltrated in embedding resin
480 medium (#T028, TAAB, UK) for 4 h at room temperature. Next, the samples were
481 embedded on flat moulds and polymerised at 70°C for 24 h. Ultrathin sections (100-120
482 nm) were cut on a Leica ultramicrotome (Leica microsystems, Germany) and mounted
483 on mesh copper grids. They were contrasted with uranyl acetate for 2 minutes and with
484 lead citrate for 1 minute. Finally, the sections were imaged on an EM-1400 (Plus)
485 transmission microscope operated at 120 kV (JEOL USA, Inc.). For each section of each
486 brain region (frontal cortex, caudate, putamen), 5 to 10 pictures were examined for
487 pathological changes in the capillary and neurovascular unit. The original dimensions of
488 the images are 3296x2472 pixels.
489
490 The presence of a single layer of endothelial cell surrounded by a layer of basement
491 membrane was considered to be an intact capillary. The observation of oedematous
492 space and vacuoles around the vessels, vacuolated pericytes, large vacuoles in the
493 endothelial cells or endoplasmic reticulum swelling, as well as oedema around the
494 capillary and multiple layers of basement membrane were considered as signs of
495 pathological changes (46). Neurodegeneration was identified by the presence of
496 lipofuscin granules, loss of myelin compactness, neurite degeneration and fibrillary
497 deposits (47,48).

498

499 **Western blot studies**

500 Post-mortem brain capillaries from neurologically healthy individuals and AD cases
501 were used to investigate the expression of transporters. The Braak stage of the control
502 cases was between I, and II (age-related pathology only). For the AD cases, the Braak
503 stage was between IV and VI. See Supplementary Information about the sex, age, post-
504 mortem delay (PMD), clinical diagnosis, and Braak stage of the individual cases
505 (Supplementary Table 2, S1 File).

506

507 Brain capillaries isolated from healthy individuals and AD patients were used to
508 investigate the expression levels of BBB transporters of interest by WB analysis. Brain
509 capillaries were isolated after homogenising brain tissue from the frontal cortex or the
510 caudate and carrying out a dextran-based density-gradient centrifugation to produce a
511 capillary enriched pellet. The capillary pellet was then homogenised in capillary
512 depletion buffer (brain weight x 3) and 26% dextran (brain weight x 4). The homogenate
513 was subjected to density gradient centrifugation (5,400 G for 15 minutes at 4°C) to give
514 an endothelial cell-enriched pellet, the resulting supernatant was discarded (49). The
515 pellet was further lysed in 150-200 µl ice-cold RIPA buffer with added protease
516 inhibitors at 4°C, and then centrifuged at 8,000 G for 15 minutes at 4°C.

517

518 The protein concentration in each lysate was determined using a BCA assay and the WB
519 procedure was carried out as already described. For antibodies used, see Supplementary
520 Table 1, S1 File.

521

522 We used anti-TfR1 antibodies to detect TfR1 - an endothelial cell marker. This way we
523 aimed to confirm that the capillary pellets were enriched in endothelial cells. We also
524 used antibodies to detect GLUT1, and P-gp.

525

526 Quantification of protein expression was determined by calculating the intensity ratio of
527 the band of interest and the band of the loading control (GAPDH). Band intensity ratio
528 analysis was conducted using ImageJ software (35).

529

530 For statistical analysis, we used two-tailed unpaired Student's t-test to compare the
531 difference of transporter expression in the frontal cortex and the caudate between control
532 and AD cases.

533

534 Results

535 Physicochemical characteristics of amisulpride and glucose

536 We determined the physicochemical characteristics of amisulpride and D-glucose using
537 DrugBank and MarvinSketch. Amisulpride (chemical abstracts service (CAS) number
538 71675-85-9) has a MW of 369.48 g/mol, a pKa of 9.37 and exists as two microspecies at
539 physiological pH. The predominant (96.77%) microspecies is positively charged and
540 has a single positive charge at pH 7.4. The other microspecies (3.23%) has no charge
541 (Fig 1). The gross charge distribution at pH 7.4 of amisulpride is +0.968.

542

543 **Fig 1. The percentage distribution and chemical structures of the two amisulpride**
544 **microspecies found at physiological pH.** Microspecies A has a single positive charge
545 and Microspecies B has no charge, according to MarvinSketch 22.9.0.
546
547 D-glucose has a MW of 180.16 g/mol, and a pKa of 11.8. In solution, at equilibrium, D-
548 glucose exists as two anomers that interconvert spontaneously: ~36% alpha-D-glucose,
549 and ~64% beta-D-glucose, with less than 0.01% being present as an open-chain form
550 (linear glucose) (32,50). The major microspecies (99.99%) of both alpha-D-glucose and
551 beta-D-glucose has no charge (Supplementary Table 2, S1 File). The other microspecies
552 (0.01%) of each anomer has a single negative charge at physiological pH. The linear
553 form of D-glucose was found to be 100% neutral. Only alpha- and beta-D-glucose have
554 been included in the GLUT1 substrates group (Supplementary Table 2, S1 File).
555

556 # Identification of GLUT1 substrates and inhibitors

557 Our two PubMed searches identified 99 reviews, and 16 primary research articles, which
558 discussed GLUT1 substrates, GLUT1 inhibitors or antipsychotics which interacted with
559 GLUT transporters and matched our inclusion criteria. In these reviews and primary
560 research articles, 9 GLUT1 substrates, 33 GLUT1 inhibitors, and 11 GLUT-interacting
561 antipsychotics (including 6 typical antipsychotics and 5 atypical antipsychotics) were
562 described and are listed in Supplementary Table 3-5, S1 File. They include the typical
563 antipsychotics: chlorpromazine, fluphenazine, loxapine, pimozide and spiperone.
564 Haloperidol is also included although some studies suggest no interaction with GLUT
565 (23)(51). Atypical antipsychotics include: clozapine, desmethylclozapine, olanzapine,

566 quetiapine and risperidone. Supplementary Table 6 (S1 File) provides specific details
567 about the experimental evidence that indicates that these 11 antipsychotics interact with
568 GLUT. In all cases this interaction was considered to be inhibitory.
569

570 Physicochemical characteristics of published substrates and 571 inhibitors of GLUT1

572 Molecular Weight

573 The physiochemical characteristics of the identified GLUT1 substrates, GLUT1
574 inhibitors and the antipsychotics that interact with GLUT are summarised and compared
575 to amisulpride (Fig 2, Table 1, and Supplementary Table 3-5, S1 File). The MW range
576 for the GLUT1 substrates was 164.16 g/mol to 232.28 g/mol, with a mean±SEM of
577 184.95±6.45 g/mol, the MW range of the GLUT1 inhibitors was 180.16 g/mol to 518.55
578 g/mol with a mean±SEM of 325.50±14.4 g/mol and the MW range for GLUT interacting
579 antipsychotics was 312.44 to 461.55 g/ mol with a mean±SEM of 369.38±16.04 g/mol
580 (Table 1). One-way ANOVA showed differences in the MW $F(2, 50) = 18.72$, Tukey's
581 multiple comparisons test showed significant difference between the MW of GLUT1
582 substrates and inhibitors ($p<0.0001$), and between GLUT1 substrates and antipsychotics
583 ($p<0.0001$) (Fig 2A). No significant difference was observed between the MW of the
584 GLUT1 inhibitors and the group of antipsychotics (Fig 2A).
585

586 **Fig 2. Physicochemical characteristics of GLUT1 substrates and inhibitors.**
587 Evaluation of the PubMed database identified 9 substrates and 33 inhibitors of GLUT1,
588 and 11 antipsychotics inhibiting cell entry of GLUT1 substrates. A) Comparison of the

589 molecular weight (g/mol) of substrates, inhibitors of GLUT1, and antipsychotics. Each
590 square, dot, and triangle represents a compound. Comparison of the predicted gross
591 charge of substrates, inhibitors of GLUT1, and antipsychotics at pH=7.4, according to
592 MarvinSketch 22.9.0. Data was analysed using One-way ANOVA, GraphPad Prism 9.
593 B) The pie charts show the molecular weight of the substrates and inhibitors of GLUT1,
594 and of antipsychotics inhibiting cell entry of GLUT1 substrates. C) The pie charts show
595 the charge of the most prevalent microspecies of the GLUT1 substrates, inhibitors, and
596 antipsychotics interacting with GLUT at physiological pH according to MarvinSketch
597 22.9.0.
598
599 The median for the GLUT1 substrates was 180.16 g/mol, for the GLUT1 inhibitors it
600 was 308.34 g/mol, for the antipsychotics it was 375.86 g/mol (Table 1). We found that
601 88.89% of the GLUT1 substrates were small molecules with a MW between 101 and 200
602 g/mol (Fig 2B). The GLUT1 inhibitors showed a wider range of molecular weight with
603 the majority falling (69.7 %) between 250 and 400 g/mol (Figure 2B). The majority
604 (72.73%%) of the antipsychotics affecting GLUT1 substrates uptake were in the range
605 of 301-400 g/mol (Fig 2B). There was no significant difference in the molecular weight
606 between the typical (386.18±23.42) and the atypical antipsychotics (349.21±20.14)
607 (t=1.169, df=9, p= 0.27, two-tailed unpaired t-test).
608
609
610

611 **Table 1: Summary of the MW range, Mean±SEM, Median (g/mol), and gross charge at**

612 **physiological pH of GLUT1 substrates, inhibitors, and antipsychotics interacting with GLUT.**

	GLUT1 substrates n=9	GLUT1 inhibitors n=33	Antipsychotics n=11		
			All	Typical n=6	Atypical n=5
MW Range (g/mol)	164.16-232.28	180.16-518.55	312.44-461.55	318.86-461.55	312.44-410.49
Mean ± SEM (g/mol)	184.95±6.45	325.50±14.4	369.38±16.04	386.18±23.42	349.21±20.14
Median (g/mol)	180.16	308.34	375.86	385.76	326.82
Gross charge at physiological pH	+0.089 ± 0.09	-0.30 ±0.06	+0.89 ±0.02	+0.90 ±0.02	+0.87 ±0.05

613

614 ## Charge

615 We investigated the predicted gross charge distribution at physiological pH of the
616 identified substrates and inhibitors of GLUT1 as well as the GLUT interacting
617 antipsychotics (Fig 2A), and also reported the predicted charge and the percentage
618 distribution of the top two microspecies (Supplementary Table3-5, S1 File).

619

620 Overall, we found that GLUT1 substrates, GLUT1 inhibitors and GLUT-interacting
621 antipsychotics had an average gross charge distribution at pH 7.4 of +0.089±0.09,
622 -0.30±0.06, and +0.89±0.02, respectively (Fig 2A, and Table 1). There was a significant
623 difference between all three groups (One-way ANOVA $F(2,50) = 58.96$, $p<0.0001$,
624 Tukey's multiple comparisons test GLUT1 substrates vs GLUT1 inhibitors ($p=0.0057$);
625 GLUT1 substrates vs antipsychotics $p<0.0001$; GLUT1 inhibitors vs antipsychotics
626 $p<0.0001$). There was no significant difference in the gross charge between the typical
627 (0.90±0.02) and the atypical (0.87±0.05) antipsychotics ($t=0.678$, $df=9$, $p= 0.5147$, two-
628 tailed unpaired t-test).

629

630 Importantly, there were two molecules which could be outliers within their groups. This
631 included the GLUT1 substrate, glucosamine, which had a much greater charge of +0.827,
632 and the atypical antipsychotic, quetiapine, which had a lower charge of +0.696 (Fig 2A).
633
634 GLUT1 substrates existed as either one, two or three microspecies at physiological pH.
635 GLUT1 inhibitors could exist as non-ionizable molecules (e.g. mercuric chloride) or as
636 up to 25 microspecies (e.g. morin) at physiological pH. The antipsychotics suggested
637 to interact with GLUT existed at physiological pH as either two, three or four
638 microspecies. This information plus the predicted charge of the top two microspecies (if
639 present) at physiological pH is tabulated in Supplementary Tables 3-5, S1 File. The
640 charge of the major microspecies of each group is presented in the form of pie charts (Fig
641 2C). The major microspecies of GLUT1 substrates were neutral or had +1 charge, GLUT
642 inhibitors were neutral or had -1 charge and the anti-psychotics which interacted with
643 GLUT all had +1 charge at physiological pH.
644

645 *In silico* molecular docking

646 *In silico* molecular docking studies revealed that amisulpride could interact with GLUT1
647 based on the low free energy binding of the interaction: -29.04 kcal/mol, and the high
648 chem score: 26.79. The molecular docking predicted conventional hydrogen bonds
649 between oxygen atoms from amisulpride and the amino acids: threonine (THR) A: 137,
650 and tryptophan (TRP) A: 412, and between hydrogen atom in the NH_2 group of
651 amisulpride and asparagine (ASN) A: 411. Alkyl interaction between amisulpride and

652 the amino isoleucine (ILE) A: 164, and pi-pi stacking interaction between amisulpride
653 and TRP A: 412 were also observed (Fig 3A).
654
655 **Fig 3. Molecular level interactions of amisulpride, alpha-D-glucose, beta-D-glucose,**
656 **and sucrose with the binding sites of GLUT1.** 2D (left) and 3D (right) representations.
657 In the 2D representations, green dotted lines are used to show hydrogen bonds, pink
658 dotted lines are used to depict hydrophobic interactions. A) Stick representation is used
659 for amisulpride, and line representation for the amino acid residues from GLUT1. B)
660 Stick representation is used for alpha-D-glucose, and line representation for the amino
661 acid residues from GLUT1. C) Stick representation is used for beta-D-glucose, and line
662 representation for the amino acid residues from GLUT1. D) Stick representation is used
663 for sucrose, and line representation for the amino acid residues from GLUT1.
664
665 We also studied the interaction of GLUT1 with alpha-D-glucose and beta-D-glucose.
666 This interaction was used as a positive control. Molecular docking study found that both
667 alpha-D-glucose, and beta-D-glucose are substrates for GLUT1 with free binding energy
668 of -15.39 kcal/mol and chem score of 15.29. Conventional hydrogen bonds between
669 alpha-D-glucose and beta-D-glucose, and GLUT1 were observed at TRP A: 388,
670 glutamine (GLN) A: 282, ASN A: 411, and THR A: 137 (Fig 3B and 3C). The negative
671 control sucrose, a disaccharide, showed higher free binding energy and lower chem score
672 than amisulpride, and alpha- and beta-D-glucose (monosaccharide). The free energy
673 binding for the interaction of sucrose with GLUT1 was -8.58 kcal/mol, and the chem
674 score was 6.55 (Fig 3D).
675

676 # Expression and Function of GLUT1 in hCMEC/D3 cells

677 We examined the expression and function of GLUT1 in an established cell model of the
678 human BBB - the hCMEC/D3 immortalised cell line. Verification studies of the
679 experimental design were also performed.

680 ## Expression of GLUT1 in hCMEC/D3 cells

681 The hCMEC/D3 cells were found to express the GLUT1 transporter (40-60 kDa).
682 GAPDH was used as a loading control. Lysates from human colon adenocarcinoma
683 (Caco-2) cells were used as a positive control, and lysate from the human lung cancer
684 cell line (Calu-3) or human embryonic kidney cell line (HEK-293) were used as a
685 negative control (Fig 4A).

686

687 **Fig 4. Function of GLUT1 in hCMEC/D3 cells – self inhibition**. A) GLUT1
688 expression in hCMEC/D3 cells. Three passages of hCMEC/D3 cells (P30, 31, 33) (30
689 µg of protein per well) were tested for GLUT1 (40-60 kDa) expression. The figure is an
690 example membrane of three technical repeats. Caco-2 cell lysate was used as a positive
691 control; HEK-293 cell lysate was used as a negative control. GAPDH (37 kDa) was used
692 as a loading control. Antibodies used: anti-GLUT1 antibody – 1:100 000, #ab115730;
693 anti-GAPDH antibody – 1:2500, #ab9485, Abcam; secondary anti-rabbit IgG, HRP-
694 linked antibody – 1:2000, #7074, Cell Signalling Technology. B) V_d of [^{3}H]mannitol was
695 not significantly different between the control and the experimental conditions. C) Non-
696 labelled glucose decreased significantly the accumulation of [^{14}C]D-glucose
697 ([^{3}H]mannitol corrected) in hCMEC/D3 cells after 1 h of incubation. Results are
698 expressed as mean ± SEM, n=3-4 plates, passages (P33, 34, and 35) with five well

699 replicates per treatment in each plate. Data were analysed with an unpaired one-tailed
700 Student's t-test, using GraphPad Prism 9, each point represents a plate.
701

702 Accumulation assays – function of GLUT1 in hCMEC/D3 cells

703 To check that excess concentrations of D-glucose did not affect the membrane integrity
704 of the hCMEC/D3 cells, verification studies were performed. Cells were incubated with
705 [^{14}C]D-glucose and [^{3}H]mannitol as a control (containing the standard amount of non-
706 labelled D-glucose – 1.1 mM), and with [^{14}C]D-glucose, [^{3}H]mannitol, and non-labelled
707 D-glucose (4 mM) as a test condition. There was no significant change in the
708 permeability of [^{3}H]mannitol (cell permeability marker) when the cells were treated with
709 4 mM non-labelled D-glucose for 1 h (Fig 4B). Further analysis and studies could
710 therefore be performed using similar D-glucose concentrations.
711
712 To investigate the function of GLUT1 in hCMEC/D3 cells, we performed a self-
713 inhibition experiment. Incubation of the cells with 4 mM non-labelled D-glucose for 1 h
714 led to a significant decrease in the V_d of [^{14}C]D-glucose ([^{3}H]mannitol and protein
715 corrected) (from 97.5 ± 22.3 µl/mg to 37.3 ±10.8 µl/mg; t=2.161, df=5, p= 0.0415,
716 unpaired one-tailed Student's t-test, data is presented as mean ± SEM) (Fig 4C).

717 When we tested the interaction of amisulpride with GLUT1 in hCMEC/D3 cells, the
718 entry of [^{3}H]mannitol (0.05 µM) into the cells was used as a cell integrity marker. There
719 was no significant change in the [^{3}H]mannitol permeability when the cells were treated
720 with amisulpride (20, 50, or 100 µM) (Fig 5A). There was also no significant effect on

721 the V_d of [^{14}C]D-glucose when the cells were treated with amisulpride (20, 50, or 100
722 μM) (Fig 5B).
723
724 **Fig 5. Interaction of amisulpride with GLUT1 in hCMEC/D3 cells.** A) Amisulpride
725 at three different concentrations (20, 50, or 100 μM) did not have a significant effect on
726 the accumulation of [^{3}H]mannitol in hCMEC/D3 cells after 1 h of incubation. B)
727 Amisulpride at three different concentrations (20, 50, or 100 μM) did not have a
728 significant effect on the accumulation of [^{14}C]glucose ([^{3}H]mannitol corrected) in
729 hCMEC/D3 cells after 1 h of incubation. Results are expressed as mean ± SEM, n=3-4
730 plates, passages (P33, 34, and 35) with five well replicates per treatment in each plate.
731 Data were analysed with a One-way ANOVA, using GraphPad Prism 9, each point
732 represents a plate.
733

734 Animal model of AD - validation

735 Mouse weight comparison

736 We compared the weight of the WT and 5xFAD mice and of the two sexes (age between
737 12 and 15 months). All data are presented as mean ± SEM. The WT mice had higher
738 average weight than the 5xFAD mice (32.31 ± 2.93 g vs 26.15 ± 2.5 g), and all the 5xFAD
739 mice with weight lower than 25 g were female. We observed that the females had
740 significantly lower weight (g) than the males in the 5xFAD group (19.7 ± 1.46 vs 31 ±
741 1.61; t=4.983, df=5, p=0.0042; unpaired two-tailed Student's t-test). In the WT group,
742 weight difference between the sexes was smaller and did not reach significance
743 (Supplementary Fig 3, S1 File).

744

745 ## TEM ultrastructural study

746 We examined frontal cortex samples of WT and 5xFAD mice for the presence of Aβ
747 plaques using TEM. Structures were identified as Aβ plaques by comparison to Aβ
748 plaques which had previously been identified in TEM images (40). Amyloid plaques
749 were not observed in the frontal cortex of the young WT mice (4.5-6 months; weight
750 25.4 g, 26.1 g). Importantly, structures identical to Aβ plaques previously reported in the
751 literature (40) were present in the 5xFAD mice in both the young (6 months; weight 23.8
752 g, 23.5g) and the old (12 months 21.9 g, 22 g, data not shown) group (Fig 6).

753 **Fig 6. TEM ultrastructural study in WT and 5xFAD mice.** TEM image of the frontal
754 cortex of A) WT mouse, which is free of Aβ plaques, and B) 5xFAD mouse, with Aβ
755 plaques. Mouse age – 4.5 – 6 months. Magnification – 1200x, scale bar – 10 μm, n=2
756 mice per group.

757 ## Western blot studies

758 We performed WB for human APP to examine the genotype of each mouse used in this
759 study. APP is the precursor protein from which amyloid-β (Aβ) is cleaved by β-secretase
760 and γ-secretase (52). Our studies confirmed human APP expression was not detectable
761 in the WT mice, but was detectable in the 5xFAD mice cerebral capillaries (See
762 Supplementary Fig 4, S1 File)

763 We observed TfR1 and transporter expression in the mouse brain endothelial cell lysates
764 from WT and 5xFAD mice used in the *in situ* brain perfusions (See Supplementary Fig

765 5, S1 File). Thus, these experiments confirmed we have successfully isolated the BBB
766 compartment from the whole brain.

767 In particular, brain capillaries from WT and 5xFAD mice were found to express GLUT1,
768 PMAT, multi-drug and toxin extrusion protein 1 (MATE1), OCT1, and P-gp. No
769 significant effect of the genotype was found on the expression of these proteins (See
770 Supplementary Figs 5-9, S1 File).
771

772 *In situ* brain perfusions

773 [^{3}H]amisulpride uptake (uncorrected for [^{14}C]sucrose) was significantly greater than
774 [^{14}C]sucrose uptake in all brain areas studied apart from the hypothalamus, thalamus, and
775 capillary pellet in the WT mice (paired two-tailed t-test, data not shown). In the 5xFAD
776 mice the [^{3}H]amisulpride uptake (uncorrected for [^{14}C]sucrose) was significantly greater
777 than [^{14}C]sucrose uptake in all brain areas studied (paired two-tailed t-test, data not
778 shown).
779

780 When comparing WT and 5xFAD mice, there was a trend for an increase in
781 [^{3}H]amisulpride uptake into specific brain regions, whole brain homogenate, and
782 capillary pellet in the 5xFAD mice but this failed to reach statistical significance (Fig 7A
783 and 7B). However, there was a statistically significant increase in the uptake of
784 radiolabelled amisulpride in the supernatant (made of brain parenchyma and interstitial
785 fluid) of 5xFAD mice compared to WT mice ($t=2.550$, $df=8$, $p=0.0342$, unpaired two-
786 tailed t-test, by 104.86%). These results were [^{14}C]sucrose corrected. None of the regions

787 showed a significant difference in the [^{14}C]sucrose uptake between the WT and the
788 5xFAD mice (Fig 7A and 7B).
789
790 **Fig 7. [^{3}H]Amisulpride (sucrose corrected) and [^{14}C]sucrose uptake into the brain**
791 **of WT and 5xFAD mice.** WT and 5xFAD mice were perfused with [^{3}H]amisulpride and
792 [^{14}C]sucrose. Perfusion time - 10 minutes, fluid flow rate – 5.5 ml/min. Mouse age: 12-
793 15 months. WT n=6, 5xFAD n=4, apart for the hypothalamus where WT n=5, 5xFAD
794 n=4; the capillary pellet where WT n=3, 5xFAD n=3, and the homogenate where WT
795 n=6, 5xFAD n=3. No significant differences in paracellular permeability and membrane
796 integrity were observed in any region. Each dot represents data from one mouse. All data
797 are expressed as mean ± SEM, Mixed effects analysis and unpaired two-tailed Student's
798 t-test, GraphPad Prism 9.
799

800 # Human control and AD tissue studies

801 ## TEM ultrastructural study

802 For each brain region (frontal cortex, caudate, putamen), 10 to 20 pictures were
803 examined, and the endothelial cells, basement membranes, capillary lumens, axons,
804 myelin sheets and markers of degeneration were identified and labelled with reference
805 to Electron Microscopic Atlas of cells, tissues and organs (43). We observed thickened
806 basement membrane, vacuolisation of the endothelial cell, fibrillary deposits, and
807 oedema around brain capillaries in the frontal cortex, caudate and the putamen (Fig 8).
808 Various other features of degeneration were observed in our AD case (BNE stage VI),

809 including: lipofuscin granules in the frontal cortex and the putamen, and myelin
810 degeneration in the caudate (Fig 9).
811
812 **Fig 8. TEM image of capillaries in the frontal cortex (A) putamen (B) and caudate**
813 **(C) of a human AD case**. Frontal cortex and caudate magnification – 3000x scale bar –
814 2 µm. Putamen magnification – 2000x, scale bar – 5 µm. n=1 case, two sections per brain
815 area were stained and imaged, 5 to 10 images were examined per section. Case number:
816 BBN002.32856; Sex: F; Age: 74; PM delay: 19 h; Alzheimer's disease, BNE stage VI.
817
818 **Fig 9. TEM image of the A) frontal cortex (A and C), putamen (B), and caudate (D)**
819 **of human AD case.**
820 A) TEM image of the frontal cortex of human AD case.
821 B) TEM image of the putamen of human AD case.
822 A and B showing electron dense and lucid portions of lipofuscin granules. Magnification
823 – 1500x, scale bar – 5 µm.
824 C) TEM image of degenerating neurites and degenerating myelinated axon in the frontal
825 cortex of a human AD case. Magnification – 6000x, scale bar – 2 µm.
826 D) TEM image of myelin and axon degeneration in the caudate of a human AD case.
827 Magnification – 2500x, scale bar – 5 µm.
828 Case, n=1, two sections per brain area were stained and imaged, 5 to 10 images were
829 examined per section. Case number: BBN002.32856; Sex: F; Age: 74; PM delay: 19 h;
830 Alzheimer's disease, BNE stage VI.
831

832 ## Total protein concentration

833 A BCA assay was used to compare the total protein concentration in the frontal cortex
834 and caudate capillary lysates of control vs AD cases. For the frontal cortex control cases
835 n=9; AD cases n=9) and caudate (control cases n=9; AD cases n=5), an unpaired two-
836 tailed t-tests showed no significant difference between AD and control (Supplementary
837 Fig 10, S1 File).

838

839 ## Western blot studies

840 TfR1 was detected in the capillary protein lysates from the frontal cortex and caudate of
841 human brains both in the control and in AD cases. There was no significant difference
842 between the two groups in the frontal cortex or the caudate (unpaired two-tailed t-test).
843 The expression of TfR1 in the samples confirms they are endothelial cell enriched (Fig
844 10).

845 **Fig 10: TfR1, GLUT1 and P-gp expression in human frontal cortex and caudate**
846 **brain capillary lysates. Comparing control and AD expression.** Intensity ratio was
847 calculated using the intensity of the band of TfR1, GLUT1 or P-gp, and controlling it for
848 the intensity of the loading control GAPDH. Results are presented as mean±SEM, each
849 dot represents a case, data was analysed using unpaired two-tailed Student's t-test. All
850 analysis was performed using Image J, Excel, and GraphPad Prism 9.

851

852 We studied the expression of GLUT1 in control and AD age-matched cases. We did not
853 see a significant change in the expression of GLUT1 between control and AD in the
854 frontal cortex or the caudate (Fig 10).

855

856 We also studied the expression of P-gp in control and AD age-matched cases. The brain
857 areas we examined were the frontal cortex and the caudate. We observed a decrease in
858 P-gp expression in the AD group comparted to control, both in the frontal cortex and the
859 caudate. In the caudate this decrease was significant (t=2.841, df=16, p=0.0118),
860 unpaired two-tailed Student's t-test (Fig 10; Supplementary Figs 11-13, S1 File).

861

862 Discussion

863 This study investigated the role of GLUT1 in the transport of the antipsychotic,
864 amisulpride at the BBB, to understand better its role in the hypersensitivity of AD
865 patients to the side effects of antipsychotics compared to healthy aged patients (4). We
866 used an integrative approach to test the hypotheses that amisulpride interacts with
867 GLUT1 at the BBB, and that expression of BBB transporters and the transport of
868 amisulpride and glucose into the brain is affected by AD. Analysis of the published
869 literature allowed us to identify three groups of molecules: GLUT1 substrates, GLUT1
870 inhibitors and antipsychotics that interacted with GLUT. We then utilized specialist
871 chemical property databases to obtain a clearer picture of the physicochemical
872 characteristics of these molecules and their groups as well as amisulpride. *In silico*
873 docking studies allowed us to explore the specific molecular interactions of amisulpride
874 with GLUT1. WB and *in vitro* accumulation assays in hCMEC/D3 cells were used to
875 confirm the expression of GLUT1 protein in these BBB cells, the presence of functional
876 GLUT1 transporter, and to determine possible interactions between GLUT1 and
877 amisulpride. We also examined the neurovascular unit architecture in WT and 5xFAD

878 mice at an ultrastructural level using TEM and assessed the suitability of the 5xFAD
879 mouse model to study the BBB permeability of amisulpride in AD. WB was used to
880 study the expression of SLC and ABC transporters, including GLUT1 at the BBB in WT
881 and 5xFAD mice. The *in situ* brain perfusion technique allowed us to compare
882 amisulpride uptake into compartments of the brain in WT and 5xFAD mice. We also
883 compared transporter expression in capillaries from human cases with and without
884 Alzheimer's dementia. TEM was utilised to directly visualise cellular structures in an
885 individual with AD.
886

887 Physicochemical characteristics of GLUT1 substrates and 888 inhibitors

889 Amisulpride is an atypical antipsychotic and has a MW of 369.48 g/mol. The main
890 microspecies (96.77%) at physiological pH has one positive charge. The other
891 microspecies (3.23%) of amisulpride at physiological pH has no charge. The gross
892 charge distribution at pH 7.4 of amisulpride is +0.968.
893

894 Our literature review and analysis of the chemical property databases revealed that
895 GLUT1 substrates are typically neutral, however, we have identified one substrate, D-
896 glucosamine, which has a positive gross charge distribution physiological pH of +0.827.
897 GLUT1 inhibitors are predominately neutral, but we identified inhibitors which had a
898 negative gross charge distribution at pH 7.4 (for example, -1.043 - Lavendustin B).
899

900 Importantly, both typical and atypical antipsychotics were identified which impede
901 uptake of GLUT1 substrates *in vitro*. They all have a gross charge distribution which is
902 positive at physiological pH and their main microspecies at physiological pH has a single
903 positive charge, similar to amisulpride. An example is olanzapine for which there is also
904 *in silico* molecular docking data for an inhibitory interaction with a bacterial glucose/H^+
905 symporter from *Staphylococcus epidermidis*. It can impede the alternating opening and
906 closing of the substrate cavity necessary for glucose transport (53). Another example is
907 risperidone (24), which has been reported to interact with GLUT, and to inhibit glucose
908 uptake *in vitro* (in rat PC12 cells). Thus, it is plausible that other atypical antipsychotics
909 such as amisulpride could interact with GLUT1.
910
911 Although it is important to consider that not all antipsychotics interact with GLUT. For
912 example, sulpiride (CAS 23756-79-8; MW 341.43, gross charge at physiological pH
913 +0.972) and clozapine N-oxide (a clozapine metabolite: CAS 34233-69-7; MW 342.83,
914 gross charge at physiological pH +1.616) were reported to not have a significant effect
915 on glucose uptake *in vitro* (23,51).
916
917 When it comes to MW, all the established substrates of GLUT1 are smaller than
918 amisulpride – 164.16 to 232.28 g/mol (MW of the main substrate - glucose is 180.16
919 g/mol). Amisulpride, has a MW similar to the established GLUT1 inhibitors and to the
920 antipsychotics reported to inhibit uptake of GLUT1 substrates. Amisulpride is therefore
921 more likely to represent a GLUT1 inhibitor than substrate. However, this interpretation
922 is limited by the small number of established GLUT1 substrates, even though a large
923 number of reviews (99) were examined.

924

925 First generation antipsychotics are known to inhibit dopaminergic neurotransmission
926 most effectively by blocking about 72% of the D2 dopamine receptors in the brain. They
927 also block noradrenergic, cholinergic, and histaminergic receptors. Whereas, second
928 generation antipsychotics block D2 dopamine receptors and serotonin receptors (5-HT),
929 mainly the 5-HT2A subtype (54).

930

931 Interestingly, amisulpride (second generation antipsychotic) shows high and similar
932 affinities for the D2 and D3 dopamine receptor subtypes but it does not have significant
933 affinity to the other receptor subtypes (55).

934

935 Although atypical antipsychotics are usually considered to have a broader mechanism of
936 action compared to typical antipsychotics, there were no significant differences in
937 physicochemical characteristics of the two groups or in their reported type of interaction
938 with GLUT1.

939

940 *In silico* studies

941 *In silico*, GLUT1 was found to interact with amisulpride with a free energy binding of -
942 29.04 kcal/mol (the positive control, beta-D-glucose, showed free energy binding of -
943 15.39 kcal/mol, and the negative control, sucrose, showed much higher free energy
944 binding of -8.58 kcal/mol). Previous studies have shown that interactions with TRP412,
945 TRP388, phenylalanine (PHE) 291, PHE379 and glutamate (GLU) 380 may play critical
946 roles in ligand binding to GLUT1 in the inward open conformation (33). Also, another

947 study reported interactions between cytochalasin B, a competitive inhibitor of glucose
948 exit via GLUT1 (56), and THR137, ASN411, GLN282, ASN288, glycine (GLY) 384
949 and TRP388 in GLUT1 (57). In addition, ASN411 and TRP412 were found to be
950 important for the binding of inhibitors in the central binding site of GLUT1 (57).
951 Importantly, we see interactions between amisulpride and GLUT1 at some of the
952 reported amino acid residues – TRP412, THR137 and ASN411. The interaction of
953 amisulpride with these specific amino acid residues in GLUT1, taken together with the
954 size of amisulpride compared to GLUT1 substrates and inhibitors, and its positive
955 charge, suggests amisulpride might competitively inhibit glucose delivery to the CNS
956 via GLUT1.
957
958 Dysfunction of GLUT1 is likely to cause further dysregulation of the neurovascular unit
959 (NVU), resulting in the loss of BBB integrity as well as the observed altered transporter
960 expression and increased Aβ toxicity in AD. Interestingly, increased neuronal uptake of
961 glucose has been shown to protect against Aβ toxicity, and altering glucose delivery to
962 the brain could influence progression of AD pathology (58). A situation that may be
963 exacerbated by the additional medications AD patients usually receive (59).
964 Antipsychotics are commonly prescribed with antidepressant or sedative drugs (60), i.e.,
965 citalopram (2) (MW: 324.4; +1 charge at pH 7.4) (30). It can be assumed that if two of
966 these psychotropics are substrates (or inhibitors) for the same transporter and are
967 prescribed together then this is likely to change individual drug delivery and potentially
968 nutrient delivery to the CNS and contribute to the drug hypersensitivity. In fact,
969 polypharmacy is an important predictor of adverse drug reactions for people with and
970 without dementia (59).

971

972 ## *In vitro* studies in model of the human BBB (hCMEC/D3 cells)

973 We confirmed the expression of GLUT1 in the hCMEC/D3 cells with WBs. These results
974 are in line with previous studies. GLUT1 protein expression has been detected in
975 hCMEC/D3 cells and in brain microvascular endothelial cells derived from healthy
976 patient-derived induced pluripotent stem cells (61,62). Other glucose transporters'
977 mRNA has also been detected in the hCMEC/D3 cells, namely GLUT3 and sodium-
978 dependent glucose transporter 1 (SGLT1) (62,63). Protein expression of GLUT3 and
979 GLUT4, but not SGLT1, has also been reported in hCMEC/D3 cells (61). Nevertheless,
980 there is consensus that GLUT1 is the most highly expressed transporter in the
981 hCMEC/D3 cells and the BBB (64).

982

983 *In vitro*, our self-inhibition study using 4 mM non-labelled glucose, showed that 4 mM
984 glucose significantly decreased the uptake of [^{14}C]D-glucose into the hCMEC/D3 cells
985 but did not affect membrane integrity as measured with [^{3}H]mannitol. This suggests the
986 presence of functional glucose transporter on the hCMEC/D3 cells.

987

988 Our *in vitro* experiments looking at the interaction between antipsychotics and GLUT1
989 showed no effect of micromolar concentrations of amisulpride on the accumulation of
990 [^{14}C]D-glucose into the hCMEC/D3 cells. This suggests that clinically relevant
991 concentrations of amisulpride do not inhibit GLUT1 (amisulpride has a plasma Cmax of
992 0.17-1.19 μM) (4,65). However, these results are difficult to interpret conclusively as
993 the GLUT1 is partially saturated due to the presence of non-labelled glucose in the

994 control accumulation assay buffer. The non-labelled glucose being essential for
995 endothelial cell survival.
996
997 Overall, the high affinity (Km = ~2mM (66)) of the GLUT1 transporter, high expression
998 of GLUT1 at the BBB, excess glucose concentrations in buffer/plasma and the low
999 concentrations of amisulpride could make the interaction between amisulpride and
1000 GLUT1 difficult to detect *in vitro.* Amisulpride has been associated with hyperglycemia
1001 as a side effect in 1 in 100 people (67). The hyperglycaemia possibly being caused by
1002 inhibition of GLUT1 transport. Interestingly, recent studies did not associate its use with
1003 a higher prevalence of diabetes (68)
1004
1005 Cell culture studies have shown that another second-generation antipsychotic - clozapine,
1006 inhibits glucose uptake (at 20 μM) in PC12 rat cells after a 30-minute incubation.
1007 Exposure to clozapine beyond 24 h (at concentrations up to 20 μM), there was a
1008 significant increase in the cellular expression of GLUT1 and GLUT3 (23).
1009
1010 Later studies have confirmed that both clozapine and risperidone interact with glucose
1011 transporters and inhibit glucose transport. It has been suggested that this could be
1012 mediated by directly binding to glucose transporters and allosterically modulating either
1013 a glucose binding side or the conformational change in the protein conformation required
1014 for transport (24). Importantly, risperidone which is the only antipsychotics licensed for
1015 use in AD, shows treatment response and emergent side effects at very low doses and
1016 low plasma concentrations (7), similar to amisulpride (10). Also, clozapine is used at low

1017 doses and at correspondingly low plasma concentrations in the treatment of psychosis in
1018 Parkinson's disease patients (69).
1019

1020 Animal model studies in WT and 5xFamilial AD (FAD) mice

1021 In order to study the effect of AD on the BBB and how this contributes to the increased
1022 sensitivity of AD patients to antipsychotics, we need good preclinical models. In this
1023 study we utilized the 5xFAD mice. The significantly lower weight of the female mice,
1024 compared to the male mice of the 5xFAD genotype which we observed, matches with
1025 previous reports that female mice develop the pathology earlier than male mice (70). This
1026 could be related to increased expression of the Thy1 promoter which drives the
1027 transgenes in the 5xFAD mice and has an oestrogen response element (71) resulting in
1028 generation of higher levels of Aβ (72).
1029

1030 TEM ultrastructural study

1031 Using TEM, we detected Aβ plaques in the frontal cortex of 5xFAD mice from 6 months
1032 of age. This is in agreement with previous data, reporting amyloid deposition in these
1033 mice from the age of 2 months (40) and with our Western blot studies which confirmed
1034 APP expression.
1035

1036 *In situ* brain perfusions

1037 When we studied the permeability of [^{3}H]amisulpride across the BBB in a whole animal
1038 *in vivo*, we observed low permeability of the drug across the BBB in WT and in 5xFAD
1039 mice (both groups 12-15 months of age).

1040 Interestingly, as measured by [^{14}C]sucrose (MW 359.48 g/mol), there was no significant
1041 change in vascular integrity between age-matched WT and 5xFAD mice in all areas that
1042 we investigated even though there was a trend for increased permeability in the 5xFAD
1043 mice in the frontal cortex, thalamus, supernatant, and homogenate. Importantly, there
1044 was significantly higher uptake of [^{3}H]amisulpride (corrected for [^{14}C]sucrose) in the
1045 supernatant of 5xFAD mice compared to WT mice. An earlier animal study has also
1046 reported difference in the brain uptake of amisulpride in an AD mouse model compared
1047 to WT, without significant change in the [^{14}C]sucrose uptake, i.e. without significant
1048 change in BBB integrity (16). The 3xTg mouse model of AD had increased
1049 [^{3}H]amisulpride uptake in the frontal cortex, but not the occipital cortex, compared to
1050 WT mice at 24 months of age (age matched) (16). Thus, suggesting that the increased
1051 uptake of amisulpride in the brain of the 5xFAD mice could be related to regional BBB
1052 changes in transporter expression associated with AD.

1053 **Western blot studies**

1054 A decrease in GLUT1 expression in brain samples has been observed previously using
1055 WB in 5xFAD mice compared to WT at 9 months of age (73). This study used whole
1056 brain samples and pooled the samples from all of their WT mice together and from all of
1057 their 5xFAD mice together (73). In our study we confirmed the expression of GLUT1 in
1058 5xFAD and WT mouse capillaries at 12-15 months of age. We did not observe significant
1059 difference between the genotypes, this is likely related to the fact that we did not pool
1060 our samples but analysed each mouse separately which would have increased variability.
1061

1062 Other studies using the 5xFAD mouse model have reported a decrease in the expression
1063 of P-gp and GLUT1 in the cortex capillaries of 6-month-old 5xFAD mice, compared to
1064 age-matched WT mice (74). We did not detect any effect of the genotype; this could be
1065 because we used the whole mouse brain to prepare the capillary samples and to perform
1066 WB, and the expression changes could be region-specific.
1067 Finally, expression of PMAT, MATE1, OCT1, and P-gp has been reported in the BBB
1068 of 3xTg mice. No difference in expression levels was observed when they were compared
1069 to age matched WT mice (16). These results are in line with our observations in the
1070 5xFAD model. This could be because both studies used the whole brain to do capillary
1071 isolation, whereas the AD-associated transporter expression changes might be regional,
1072 as seen in human control and AD cases (16).
1073

1074 Human control and AD tissue studies

1075 TEM ultrastructural study

1076 In our AD case we were able to identify brain capillaries, myelinated axons and neurites
1077 using TEM. Our images showed signs of NVU, and brain degeneration such as swollen
1078 basement membrane and oedema around the capillaries, lipofuscin granules,
1079 degenerating neurites, degenerating myelin, and fibrillary depositions.
1080
1081 Previous EM studies have also reported abnormalities in the brain capillaries, associated
1082 with AD, these include, splitting and duplication of the basement membrane, reduction
1083 of the length of the tight junctions, morphological alterations of the mitochondria of the
1084 endothelial cells, the pericytes and the perivascular astrocytic processes. The number of

1085 the pinocytic vesicles was substantially increased in the endothelium of the brain
1086 capillaries in AD in comparison with age-matched controls. Thus, it has been suggested
1087 that abnormalities in the brain capillaries may result in the release of neurotoxic factors
1088 and abnormal Aβ homeostasis in the brain and contribute to AD pathology (75).
1089

1090 **Western blot studies**

1091 Expression of the endothelial marker TfR1 in our human brain capillary lysates confirms
1092 that we have isolated brain capillary pellets enriched in endothelial cells. There was no
1093 significant change in TfR1 expression between control and AD samples observed.
1094

1095 Diminished glucose uptake has been reported in the hippocampus, parietotemporal
1096 cortex and/or posterior cingulate cortex in individuals at genetic risk for AD (76),
1097 positive family history (77) and/or mild or no cognitive impairment who develop AD
1098 (78,79). Reduced levels of GLUT1 in cerebral microvessels have also been reported in
1099 AD in the caudate nucleus (80), frontal cortex (protein was decreased but not mRNA)
1100 (19), and the hippocampus (18). It has been suggested that GLUT1 deficiency can
1101 contribute to the disease process, acting in tandem with Aβ to initiate or amplify vascular
1102 damage and Aβ accumulation (81). We did not observe a significant change in GLUT1
1103 expression in the frontal cortex and caudate between controls and AD patients. This
1104 could be related to the insufficient selectivity of the antibody, the need of more cases, or
1105 the heterogeneity in the group of cases.
1106

1107 P-gp is ubiquitously and abundantly expressed in the brain capillaries (82). Importantly,
1108 protein expression has been reported to decrease significantly in the prefrontal cortex of
1109 AD patients, compared to healthy ageing controls (61 to 100 years old) (83). In line with
1110 other studies, we observed a decrease in the P-gp expression in the caudate capillaries of
1111 AD patients, compared to healthy controls. Importantly, P-gp protects the brain from
1112 potentially toxic substances and has been reported to extrude Aβ from the brain (84). It
1113 has been suggested that downregulation of P-gp could allow pharmaceuticals into the
1114 central nervous system and may increase the accumulation of Aβ (83).
1115

1116 Conclusion

1117 In conclusion, a literature review identified GLUT1 substrates, GLUT1 inhibitors and
1118 antipsychotics that interacted with GLUT. Physicochemical characterization of these
1119 groups using chemical property databases established that amisulpride had similar
1120 properties to the GLUT-interacting antipsychotics group. Our *in silico* molecular
1121 docking studies revealed that amisulpride interacts with GLUT1 and could potentially
1122 affect glucose delivery to the CNS. We also have *in vitro* evidence for the presence of
1123 functional glucose transporter in the hCMEC/D3 cells line. However, we could not
1124 detect any interaction of amisulpride with GLUT1 in this assay. This is possibly because
1125 glucose being essential for endothelial cell survival limits the sensitivity of this assay for
1126 exploring antipsychotic interaction with GLUT1 *in vitro*. TEM and WB analysis
1127 validated the 5xFAD mouse model for our study. The *in situ* brain perfusion studies
1128 showed limited entry of amisulpride across the BBB in both WT and 5xFAD mice, and
1129 an increased uptake into the brain of the 5xFAD mice compared to WT mice, although

1130 the cerebrovascular space was similar in both genotypes. Our WB work with P-gp further
1131 confirms that transporter expression at the human BBB is altered in AD, although a
1132 significant difference was not observed for GLUT1 expression in our cases. It is possible
1133 that amisulpride competitively inhibits glucose entry via GLUT1, which may further
1134 compromise the neurovascular unit and increase BBB permeability, and therefore
1135 increase central drug access, and contribute to the amisulpride sensitivity observed in
1136 AD. This research further confirms the national guidance that antipsychotic drugs should
1137 only be prescribed at the lowest dose possible for the shortest durations in AD. It is also
1138 plausible that, in the longer term, the impact on energy delivery to the brain may lead to
1139 further cellular degeneration. The implications of our findings extend to other
1140 antipsychotic drugs.
1141

1142 List of abbreviations

1143 3xTgAD: triple transgenic, Aβ: amyloid beta, AD model; 5xFAD: five times familial
1144 Alzheimer's disease mouse model; ABC: Adenosine triphosphate binding cassette; AD:
1145 Alzheimer's disease; APP: amyloid precursor protein; ASN: asparagine; BBB: blood–
1146 brain barrier; BCA: bicinchoninic acid; BDR: Brain for Dementia Research; dpm:
1147 disintegrations per minute; CAS: chemical abstracts service number; FBS: foetal bovine
1148 serum; GLN: glutamine; GLU: glutamate; GLUT1: glucose transporter 1; GLY: glycine;
1149 hCMEC/D3: immortalized human cerebral microvessel endothelial cell line; HEK cells:
1150 human embryonic kidney cells; MATEs: multi-drug and toxin extrusion proteins; MW:
1151 molecular weight; OCT: organic cation transporters; NVU: neurovascular unit; PFA:
1152 paraformaldehyde; P-gp: P-glycoprotein; PHE: phenylalanine; PMAT: plasma

1153 membrane monoamine transporter; PMD: post-mortem delay; RIPA: radio-
1154 immunoprecipitation assay; SGLT1: sodium-dependent glucose transporter 1; SLC:
1155 solute carrier; TEM: transmission electron microscopy; TfR1: transferrin receptor 1;
1156 THR: threonine; TRP: tryptophan; V_d: volume of distribution; WB: Western blot; WT:
1157 wild type.
1158

1159 Declarations

1160 Ethics approval and consent to practice

1161 All *in vivo* animal experiments were performed in accordance with the Animal Scientific
1162 Procedures Act (1986) and Amendment Regulations 2012 and with consideration to the
1163 Animal Research: Reporting of *In Vivo* Experiments (ARRIVE) guidelines. The study
1164 was approved by the King's College London Animal Welfare and Ethical Review Body.
1165 The UK government home office project license number was 70/7755.
1166

1167 Human tissue brain samples were provided via Brains for Dementia Research (BDR) and
1168 were anonymised. Written consent was provided by BDR and the specific BDR reference
1169 numbers were: TRID_170, TRID_170 amendment, TRID_265 and TRID_287.
1170 BDR has ethical approval granted by the National Health Service (NHS) health research
1171 authority (NRES Committee London-City & East, UK: REC reference:08/H0704/128+5.
1172 IRAS project ID:120436). Tissue samples were supplied by The Manchester Brain Bank
1173 and the London Neurodegenerative Diseases Brain Bank, which are both part of the BDR
1174 programme, jointly funded by Alzheimer's Research UK and Alzheimer's Society.

Tissue was received on the basis that it will be handled, stored, used, and disposed of within the terms of the Human Tissue Act 2004.

Consent for publication

This research was funded in whole, or in part, by the Wellcome Trust [080268]. For the purpose of Open Access, the author has applied a CC BY public copyright licence to any Author Accepted Manuscript version arising from this submission.

Availability of data and materials

The datasets supporting the conclusions of this article are included within the article and supplementary S1 File.

Competing interests

The authors declare that they have no competing interests.

Acknowledgements

We acknowledge the support of Professor D.M. Mann from the Manchester Brain Bank who provided some of the human brain tissue samples used in this study. We would also like to thank Ms S. Selvackadunco from the London Neurodegenerative Diseases Brain Bank for her assistance with acquiring the human brain samples used in our WB and

1196 TEM studies. We also acknowledge the support of Professors I. Romero, B. Weksler,

1197 and P. Couraud who provided the hCMEC/D3 cell line under MTA.

1198

1199 References

1200 1. Jeste D V, Jin H, Golshan S, Mudaliar S, Glorioso D, Fellows I, et al. Discontinuation of
1201 quetiapine from an NIMH-funded trial due to serious adverse events. Am J Psychiatry. 2009
1202 Aug;166(8):937–8.
1203 2. Jeste D V, Blazer D, Casey D, Meeks T, Salzman C, Schneider L, et al. ACNP White Paper:
1204 update on use of antipsychotic drugs in elderly persons with dementia.
1205 Neuropsychopharmacology [Internet]. 2008 Apr;33(5):957–70. Available from:
1206 http://dx.doi.org/10.1038/sj.npp.1301492
1207 3. Murray PS, Kumar S, Demichele-Sweet MAA, Sweet RA. Psychosis in Alzheimer's disease.
1208 Biol Psychiatry [Internet]. 2014 Apr;75(7):542–52. Available from:
1209 http://dx.doi.org/10.1016/j.biopsych.2013.08.020
1210 4. Reeves S, Bertrand J, D'Antonio F, McLachlan E, Nair A, Brownings S, et al. A population
1211 approach to characterise amisulpride pharmacokinetics in older people and Alzheimer's
1212 disease. Psychopharmacology (Berl) [Internet]. 2016 Sep;233(18):3371–81. Available from:
1213 http://dx.doi.org/10.1007/s00213-016-4379-6
1214 5. Ballard C, Howard R. Neuroleptic drugs in dementia: benefits and harm. Nat Rev Neurosci
1215 [Internet]. 2006 Jun;7(6):492–500. Available from: http://dx.doi.org/10.1038/nrn1926
1216 6. Schneider LS, Tariot PN, Dagerman KS, Davis SM, Hsiao JK, Ismail MS, et al.
1217 Effectiveness of atypical antipsychotic drugs in patients with Alzheimer's disease. N Engl J
1218 Med [Internet]. 2006 Oct;355(15):1525–38. Available from:
1219 http://dx.doi.org/10.1056/NEJMoa061240
1220 7. Reeves S, Bertrand J, Uchida H, Yoshida K, Otani Y, Ozer M, et al. Towards safer
1221 risperidone prescribing in Alzheimer's disease. British Journal of Psychiatry. 2021 May
1222 1;218(5):268–75.
1223 8. Schlösser R, Gründer G, Anghelescu I, Hillert A, Ewald-Gründer S, Hiemke C, et al. Long-
1224 Term Effects of the Substituted Benzamide Derivative Amisulpride on Baseline and
1225 Stimulated Prolactin Levels. Neuropsychobiology. 2002;46(1):33–40.
1226 9. Reeves S, Eggleston K, Cort E, McLachlan E, Brownings S, Nair A, et al. Therapeutic D2/3
1227 receptor occupancies and response with low amisulpride blood concentrations in very late-
1228 onset schizophrenia-like psychosis (VLOSLP). Int J Geriatr Psychiatry. 2018;33(2):396–404.
1229 10. Reeves S, Bertrand J, D'Antonio F, McLachlan E, Nair A, Brownings S, et al. A population
1230 approach to characterise amisulpride pharmacokinetics in older people and Alzheimer's
1231 disease. Psychopharmacology (Berl) [Internet]. 2016 Sep;233(18):3371–81. Available from:
1232 http://dx.doi.org/10.1007/s00213-016-4379-6
1233 11. Reeves S, McLachlan E, Bertrand J, D'Antonio F, Brownings S, Nair A, et al. Therapeutic
1234 window of dopamine D2/3 receptor occupancy to treat psychosis in Alzheimer's disease.
1235 Brain. 2017;140(4):1117–27.
1236 12. Clark-Papasavas C, Dunn JT, Greaves S, Mogg A, Gomes R, Brownings S, et al. Towards a
1237 therapeutic window of D2/3 occupancy for treatment of psychosis in Alzheimer's disease,

1238 with [18F]fallypride positron emission tomography. Int J Geriatr Psychiatry [Internet]. 2014
1239 Oct;29(10):1001–9. Available from: http://dx.doi.org/10.1002/gps.4090
1240 13. Hiemke C, Baumann P, Bergemann N, Conca A, Dietmaier O, Egberts K, et al. AGNP
1241 Consensus Guidelines for Therapeutic Drug Monitoring in Psychiatry: Update 2011.
1242 Pharmacopsychiatry. 2011 Sep;44(6):195–235.
1243 14. Lako IM, van den Heuvel ER, Knegtering H, Bruggeman R, Taxis K. Estimating dopamine
1244 D_2 receptor occupancy for doses of 8 antipsychotics: a meta-analysis. J Clin
1245 Psychopharmacol. 2013 Oct;33(5):675–81.
1246 15. Sparshatt A, Taylor D, Patel MX, Kapur S. Amisulpride - dose, plasma concentration,
1247 occupancy and response: implications for therapeutic drug monitoring. Acta Psychiatr Scand.
1248 2009 Dec;120(6):416–28.
1249 16. Sekhar GN, Fleckney AL, Boyanova ST, Rupawala H, Lo R, Wang H, et al. Region-specific
1250 blood–brain barrier transporter changes leads to increased sensitivity to amisulpride in
1251 Alzheimer's disease. Fluids Barriers CNS. 2019 Dec 17;16(1):38.
1252 17. dos Santos Pereira JN, Tadjerpisheh S, Abu Abed M, Saadatmand AR, Weksler B, Romero
1253 IA, et al. The poorly membrane permeable antipsychotic drugs amisulpride and sulpiride are
1254 substrates of the organic cation transporters from the SLC22 family. AAPS J. 2014
1255 Nov;16(6):1247–58.
1256 18. Horwood N, Davies DC. Immunolabelling of hippocampal microvessel glucose transporter
1257 protein is reduced in Alzheimer's disease. Virchows Arch. 1994;425(1):69–72.
1258 19. Mooradian AD, Chung HC, Shah GN. GLUT-1 expression in the cerebra of patients with
1259 Alzheimer's disease. Neurobiol Aging. 18(5):469–74.
1260 20. Kalaria RN, Harik SI. Reduced glucose transporter at the blood-brain barrier and in cerebral
1261 cortex in Alzheimer disease. J Neurochem. 1989 Oct;53(4):1083–8.
1262 21. Hooijmans CR, Graven C, Dederen PJ, Tanila H, van Groen T, Kiliaan AJ. Amyloid beta
1263 deposition is related to decreased glucose transporter-1 levels and hippocampal atrophy in
1264 brains of aged APP/PS1 mice. Brain Res. 2007 Nov 21;1181:93–103.
1265 22. Merlini M, Meyer EP, Ulmann-Schuler A, Nitsch RM. Vascular β-amyloid and early
1266 astrocyte alterations impair cerebrovascular function and cerebral metabolism in transgenic
1267 arcAβ mice. Acta Neuropathol. 2011 Sep;122(3):293–311.
1268 23. Dwyer DS, Pinkofsky HB, Liu Y, Bradley RJ. Antipsychotic drugs affect glucose uptake and
1269 the expression of glucose transporters in PC12 cells. Prog Neuropsychopharmacol Biol
1270 Psychiatry. 1999 Jan;23(1):69–80.
1271 24. Ardizzone TD, Bradley RJ, Freeman AM, Dwyer DS. Inhibition of glucose transport in PC12
1272 cells by the atypical antipsychotic drugs risperidone and clozapine, and structural analogs of
1273 clozapine. Brain Res [Internet]. 2001 Dec 27;923(1–2):82–90. Available from:
1274 http://www.ncbi.nlm.nih.gov/pubmed/11743975
1275 25. Lean MEJ, Pajonk FG. Patients on Atypical Antipsychotic Drugs. Diabetes Care. 2003 May
1276 1;26(5):1597–605.
1277 26. Dwyer DS, Donohoe D. Induction of hyperglycemia in mice with atypical antipsychotic
1278 drugs that inhibit glucose uptake. Pharmacol Biochem Behav. 2003 May;75(2):255–60.
1279 27. Dwyer DS, Pinkofsky HB, Liu Y, Bradley RJ. Antipsychotic drugs affect glucose uptake and
1280 the expression of glucose transporters in PC12 cells. Prog Neuropsychopharmacol Biol
1281 Psychiatry. 1999 Jan;23(1):69–80.
1282 28. Boyanova S, Wang H, Fleckney AL, Gatt A, Farag DB, Rahman KM, et al. Heightened
1283 sensitivity of people with Alzheimer's disease to the side effects of antipsychotic drug

1284 amisulpride may be mediated through an interaction with glucose transporter 1 at the
1285 blood-brain barrier. In: Alzheimer's Dement 2020;16(Suppl3):e047395. 2020.
1286 29. Bethesda (MD): National Library of Medicine (US) NC for BI. PubMed.
1287 https://pubmed.ncbi.nlm.nih.gov/ Accessed 16 March 2021.
1288 30. Wishart DS, Feunang YD, Guo AC, Lo EJ, Marcu A, Grant JR, et al. DrugBank 5.0: a major
1289 update to the DrugBank database for 2018. Nucleic Acids Res. 2018;46(D1):D1074–82.
1290 31. MarvinSketch version 22.9.0. ChemAxon http://chemaxon.com Accessed April 2022 and
1291 April 2023.
1292 32. Oliva L, Fernandez-Lopez JA, Remesar X, Alemany M. The Anomeric Nature of Glucose
1293 and Its Implications on Its Analyses and the Influence of Diet: Are Routine Glycaemia
1294 Measurements Reliable Enough? J Endocrinol Metab. 2019;9(3):63–70.
1295 33. Almahmoud S, Wang X, Vennerstrom JL, Zhong HA. Conformational Studies of Glucose
1296 Transporter 1 (GLUT1) as an Anticancer Drug Target. Molecules. 2019 Jun 7;24(11).
1297 34. Weksler BB, Subileau EA, Perrière N, Charneau P, Holloway K, Leveque M, et al. Blood-
1298 brain barrier-specific properties of a human adult brain endothelial cell line. FASEB J. 2005
1299 Nov;19(13):1872–4.
1300 35. Schneider CA, Rasband WS, Eliceiri KW. NIH Image to ImageJ: 25 years of image analysis.
1301 Vol. 9, Nature Methods. 2012. p. 671–5.
1302 36. Wolff A, Antfolk M, Brodin B, Tenje M. In Vitro Blood-Brain Barrier Models-An Overview
1303 of Established Models and New Microfluidic Approaches. J Pharm Sci. 2015
1304 Sep;104(9):2727–46.
1305 37. Cloyd JC, Snyder BD, Cleeremans B, Bundlie SR, Blomquist CH, Lakatua DJ. Mannitol
1306 pharmacokinetics and serum osmolality in dogs and humans. J Pharmacol Exp Ther. 1986
1307 Feb;236(2):301–6.
1308 38. Sprague JE, Arbeláez AM. Glucose counterregulatory responses to hypoglycemia. Pediatr
1309 Endocrinol Rev. 2011 Sep;9(1):463–73; quiz 474–5.
1310 39. Richard BC, Kurdakova A, Baches S, Bayer TA, Weggen S, Wirths O. Gene Dosage
1311 Dependent Aggravation of the Neurological Phenotype in the 5XFAD Mouse Model of
1312 Alzheimer's Disease. J Alzheimers Dis. 2015;45(4):1223–36.
1313 40. Oakley H, Cole SL, Logan S, Maus E, Shao P, Craft J, et al. Intraneuronal beta-amyloid
1314 aggregates, neurodegeneration, and neuron loss in transgenic mice with five familial
1315 Alzheimer's disease mutations: potential factors in amyloid plaque formation. J Neurosci.
1316 2006 Oct 4;26(40):10129–40.
1317 41. Rae EA, Brown RE. The problem of genotype and sex differences in life expectancy in
1318 transgenic AD mice. Neurosci Biobehav Rev. 2015 Oct;57:238–51.
1319 42. Szu J, Jullienne A, Obenaus A, Territo PR, Consortium M. Lifespan neuroimaging of the
1320 5xFAD mouse model of Alzheimer's disease: Evolution of metabolic and vascular
1321 perturbations. Alzheimer's & Dementia. 2020 Dec 7;16(S4).
1322 43. Jastrow H. Dr. Jastrows electron microscopic atlas.
1323 http://www.drjastrow.de/WAI/EM/EMAtlas.html Accessed 10 October 2019.
1324 44. Mason BL, Pariante CM, Jamel S, Thomas SA. Central Nervous System (CNS) Delivery of
1325 Glucocorticoids Is Fine-Tuned by Saturable Transporters at the Blood-CNS Barriers and
1326 Nonbarrier Regions. Endocrinology. 2010 Nov 1;151(11):5294–305.
1327 45. Báez-Mendoza R, Schultz W. The role of the striatum in social behavior. Front Neurosci.
1328 2013;7.

1329 46. Garbuzova-Davis S, Rodrigues MCO, Hernandez-Ontiveros DG, Louis MK, Willing AE,
1330 Borlongan C v, et al. Amyotrophic lateral sclerosis: a neurovascular disease. Brain Res. 2011
1331 Jun 29;1398:113–25.
1332 47. Merlo S, Nakayama ABS, Brusco J, Rossi MA, Carlotti CG, Moreira JE. Lipofuscin
1333 Granules in the Epileptic Human Temporal Neocortex with Age. Ultrastruct Pathol.
1334 2015;39(6):378–84.
1335 48. Pickett EK, Rose J, McCrory C, McKenzie CA, King D, Smith C, et al. Region-specific
1336 depletion of synaptic mitochondria in the brains of patients with Alzheimer's disease. Acta
1337 Neuropathol. 2018;136(5):747–57.
1338 49. Sanderson L, Dogruel M, Rodgers J, de Koning HP, Thomas SA. Pentamidine movement
1339 across the murine blood-brain and blood-cerebrospinal fluid barriers: effect of trypanosome
1340 infection, combination therapy, P-glycoprotein, and multidrug resistance-associated protein. J
1341 Pharmacol Exp Ther. 2009 Jun;329(3):967–77.
1342 50. Ouellette RJ, Rawn JD. Carbohydrates. In: Organic Chemistry. Elsevier; 2018. p. 889–928.
1343 51. Dwyer DS, Liu Y, Bradley RJ. Dopamine receptor antagonists modulate glucose uptake in
1344 rat pheochromocytoma (PC12) cells. Neurosci Lett. 1999 Oct;274(3):151–4.
1345 52. Chow VW, Mattson MP, Wong PC, Gleichmann M. An Overview of APP Processing
1346 Enzymes and Products. Neuromolecular Med. 2010 Mar 24;12(1):1–12.
1347 53. Babkin P, George Thompson AM, Iancu C v, Walters DE, Choe JY. Antipsychotics inhibit
1348 glucose transport: Determination of olanzapine binding site in Staphylococcus epidermidis
1349 glucose/H(+) symporter. FEBS Open Bio. 2015;5:335–40.
1350 54. Chokhawala K, Stevens L. Antipsychotic Medications [Internet]. In: StatPearls [Internet].
1351 Treasure Island (FL): StatPearls Publishing; 2023 [cited 2023 Apr 6]. Available from:
1352 https://www.ncbi.nlm.nih.gov/books/NBK519503/
1353 55. Natesan S, Reckless GE, Barlow KBL, Nobrega JN, Kapur S. Amisulpride the 'atypical'
1354 atypical antipsychotic — Comparison to haloperidol, risperidone and clozapine. Schizophr
1355 Res. 2008 Oct;105(1–3):224–35.
1356 56. Devés R, Krupka RM. Cytochalasin B and the kinetics of inhibition of biological transport. A
1357 case of asymmetric binding to the glucose carrier. Biochimica et Biophysica Acta (BBA) -
1358 Biomembranes. 1978 Jul;510(2):339–48.
1359 57. Kapoor K, Finer-Moore JS, Pedersen BP, Caboni L, Waight A, Hillig RC, et al. Mechanism
1360 of inhibition of human glucose transporter GLUT1 is conserved between cytochalasin B and
1361 phenylalanine amides. Proc Natl Acad Sci U S A. 2016 Apr 26;113(17):4711–6.
1362 58. Niccoli T, Cabecinha M, Tillmann A, Kerr F, Wong CT, Cardenes D, et al. Increased
1363 Glucose Transport into Neurons Rescues Aβ Toxicity in Drosophila. Current Biology. 2016
1364 Sep;26(17):2291–300.
1365 59. Kable A, Fullerton A, Fraser S, Palazzi K, Hullick C, Oldmeadow C, et al. Comparison of
1366 Potentially Inappropriate Medications for People with Dementia at Admission and Discharge
1367 during An Unplanned Admission to Hospital: Results from the SMS Dementia Study.
1368 Healthcare. 2019 Jan 9;7(1):8.
1369 60. Orsel K, Taipale H, Tolppanen AM, Koponen M, Tanskanen A, Tiihonen J, et al.
1370 Psychotropic drugs use and psychotropic polypharmacy among persons with Alzheimer's
1371 disease. European Neuropsychopharmacology. 2018 Nov;28(11):1260–9.
1372 61. Al-Ahmad AJ. Comparative study of expression and activity of glucose transporters between
1373 stem cell-derived brain microvascular endothelial cells and hCMEC/D3 cells. Am J Physiol
1374 Cell Physiol. 2017 Oct 1;313(4):C421–9.

1375 62. Ohtsuki S, Ikeda C, Uchida Y, Sakamoto Y, Miller F, Glacial F, et al. Quantitative targeted
1376 absolute proteomic analysis of transporters, receptors and junction proteins for validation of
1377 human cerebral microvascular endothelial cell line hCMEC/D3 as a human blood-brain
1378 barrier model. Mol Pharm. 2013 Jan 7;10(1):289–96.
1379 63. Weksler B, Romero IA, Couraud PO. The hCMEC/D3 cell line as a model of the human
1380 blood brain barrier. Fluids Barriers CNS. 2013 Mar 26;10(1):16.
1381 64. Meireles M, Martel F, Araújo J, Santos-Buelga C, Gonzalez-Manzano S, Dueñas M, et al.
1382 Characterization and modulation of glucose uptake in a human blood-brain barrier model. J
1383 Membr Biol. 2013 Sep;246(9):669–77.
1384 65. Coukell AJ, Spencer CM, Benfield P, Carpenter Tr WT. DRUG EVALUATION
1385 Amisulpride eNS A Review of its Pharmacodynamic and Pharmacokinetic Properties and
1386 Therapeutic Efficacy in the Management of Schizophrenia. Vol. 6, Drugs. 1996.
1387 66. Burant CF, Sivitz WI, Fukumoto H, Toshiaki K, Nagamatsu S, Susumo S, et al. Mammalian
1388 Glucose Transporters: Structure and Molecular Regulation. Vol. 47, RECENT PROGRESS
1389 IN HORMONE RESEARCH: Proceedings of the 1990 Laurentian Hormone Conference.
1390 1991.
1391 67. Zentiva. Patient Information Leaftlet: Amisulpride.
1392 https://www.medicines.org.uk/emc/files/pil.3965.pdf Accessed 13 January 2022.
1393 68. Holt RIG. Association Between Antipsychotic Medication Use and Diabetes. Curr Diab Rep.
1394 2019 Oct 2;19(10):96.
1395 69. Ruggieri S, de Pandis MF, Bonamartini A, Vacca L, Stocchi F. Low dose of clozapine in the
1396 treatment of dopaminergic psychosis in Parkinson's disease. Clin Neuropharmacol. 1997
1397 Jun;20(3):204–9.
1398 70. Forner S, Kawauchi S, Balderrama-Gutierrez G, Kramár EA, Matheos DP, Phan J, et al.
1399 Systematic phenotyping and characterization of the 5xFAD mouse model of Alzheimer's
1400 disease. Sci Data. 2021;8(1):270.
1401 71. Sadleir KR, Eimer WA, Cole SL, Vassar R. Aβ reduction in BACE1 heterozygous null
1402 5XFAD mice is associated with transgenic APP level. Mol Neurodegener. 2015 Jan 7;10:1.
1403 72. Maarouf CL, Kokjohn TA, Whiteside CM, Macias MP, Kalback WM, Sabbagh MN, et al.
1404 Molecular Differences and Similarities Between Alzheimer's Disease and the 5XFAD
1405 Transgenic Mouse Model of Amyloidosis. Biochem Insights. 2013;6:1–10.
1406 73. Ahn KC, Learman CR, Dunbar GL, Maiti P, Jang WC, Cha HC, et al. Characterization of
1407 Impaired Cerebrovascular Structure in APP/PS1 Mouse Brains. Neuroscience.
1408 2018;385:246–54.
1409 74. Park R, Kook SY, Park JC, Mook-Jung I. Aβ1-42 reduces P-glycoprotein in the blood-brain
1410 barrier through RAGE-NF-κB signaling. Cell Death Dis. 2014 Jun 26;5:e1299.
1411 75. Baloyannis SJ. Brain capillaries in Alzheimer's disease. Hell J Nucl Med. 18 Suppl 1:152.
1412 76. Ossenkoppele R, Prins ND, van Berckel BN. Amyloid imaging in clinical trials. Alzheimers
1413 Res Ther. 2013;5(4):36.
1414 77. Mosconi L, Rinne JO, Tsui WH, Murray J, Li Y, Glodzik L, et al. Amyloid and metabolic
1415 positron emission tomography imaging of cognitively normal adults with Alzheimer's
1416 parents. Neurobiol Aging. 2013 Jan;34(1):22–34.
1417 78. Mosconi L, Mistur R, Switalski R, Tsui WH, Glodzik L, Li Y, et al. FDG-PET changes in
1418 brain glucose metabolism from normal cognition to pathologically verified Alzheimer's
1419 disease. Eur J Nucl Med Mol Imaging. 2009 May;36(5):811–22.

79. Landau SM, Harvey D, Madison CM, Koeppe RA, Reiman EM, Foster NL, et al. Associations between cognitive, functional, and FDG-PET measures of decline in AD and MCI. Neurobiol Aging. 2011 Jul;32(7):1207–18.
80. Simpson IA, Chundu KR, Davies-Hill T, Honer WG, Davies P. Decreased concentrations of GLUT1 and GLUT3 glucose transporters in the brains of patients with Alzheimer's disease. Ann Neurol. 1994 May;35(5):546–51.
81. Winkler EA, Nishida Y, Sagare AP, Rege S v, Bell RD, Perlmutter D, et al. GLUT1 reductions exacerbate Alzheimer's disease vasculo-neuronal dysfunction and degeneration. Nat Neurosci. 2015 Apr;18(4):521–30.
82. Löscher W, Langer O. Imaging of P-glycoprotein function and expression to elucidate mechanisms of pharmacoresistance in epilepsy. Curr Top Med Chem. 2010;10(17):1785–91.
83. Chiu C, Miller MC, Monahan R, Osgood DP, Stopa EG, Silverberg GD. P-glycoprotein expression and amyloid accumulation in human aging and Alzheimer's disease: preliminary observations. Neurobiol Aging. 2015 Sep;36(9):2475–82.
84. Chai AB, Leung GKF, Callaghan R, Gelissen IC. P-glycoprotein: a role in the export of amyloid-β in Alzheimer's disease? FEBS J. 2020;287(4):612–25.

Supporting Information

- S1 File.docx

- 6 Supplementary Tables

- 13 Supplementary Figures

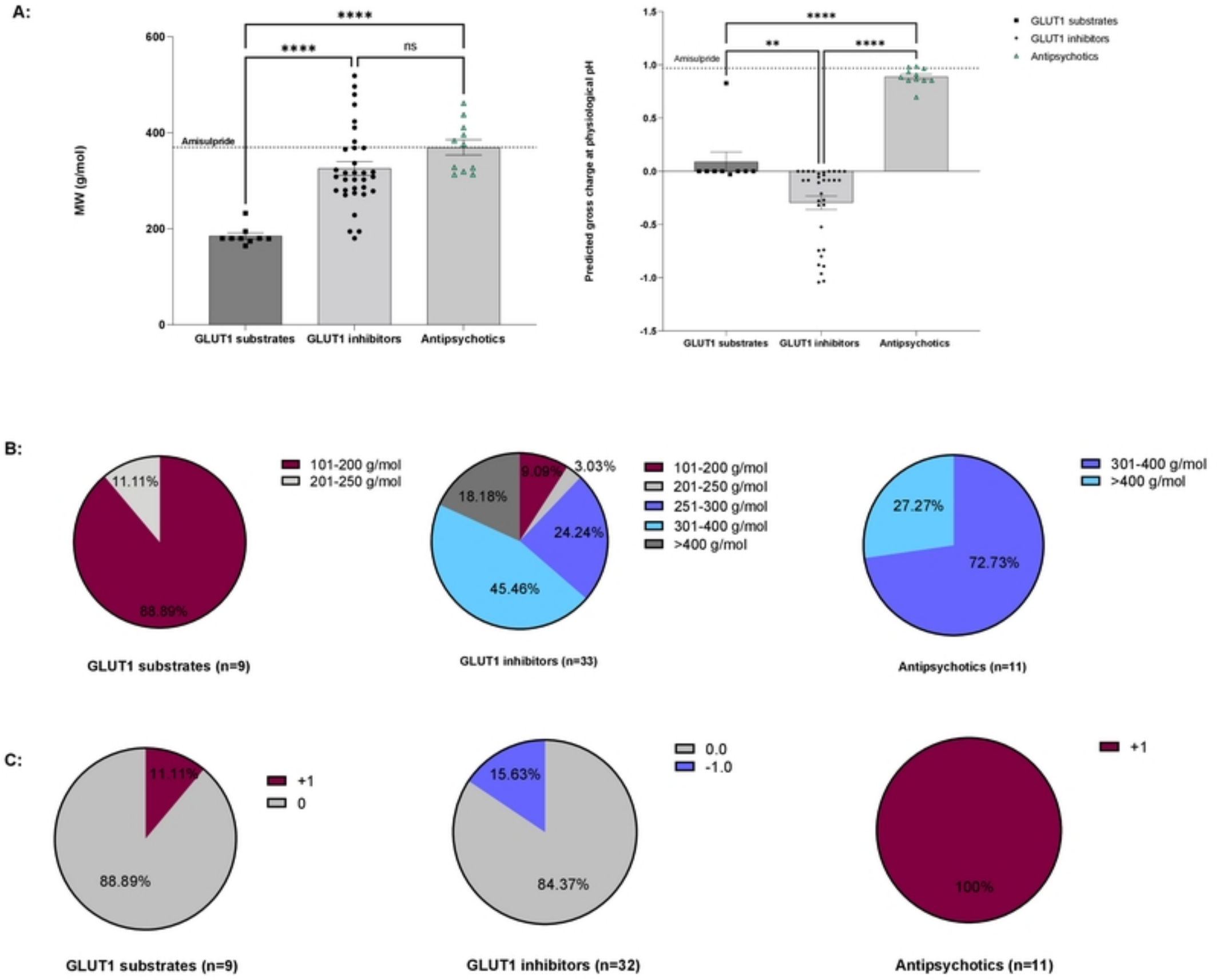
A:
MW (g/mol)
600
400
200
0
****
****
ns
Amisulpride
GLUT1 substrates
GLUT1 inhibitors
Antipsychotics
Predicted gross charge at physiological pH
1.5
1.0
0.5
0.0
-0.5
-1.0
-1.5
****
**
****
Amisulpride
GLUT1 substrates
GLUT1 inhibitors
Antipsychotics
GLUT1 substrates
GLUT1 inhibitors
Antipsychotics
B:
11.11%
88.89%
101-200 g/mol
201-250 g/mol
GLUT1 substrates (n=9)
9.09%
3.03%
18.18%
24.24%
45.46%
101-200 g/mol
201-250 g/mol
251-300 g/mol
301-400 g/mol
>400 g/mol
GLUT1 inhibitors (n=33)
27.27%
72.73%
301-400 g/mol
>400 g/mol
Antipsychotics (n=11)
C:
11.11%
88.89%
+1
0
GLUT1 substrates (n=9)
15.63%
84.37%
0.0
-1.0
GLUT1 inhibitors (n=32)
100%
+1
Antipsychotics (n=11)

Figure 2

A:

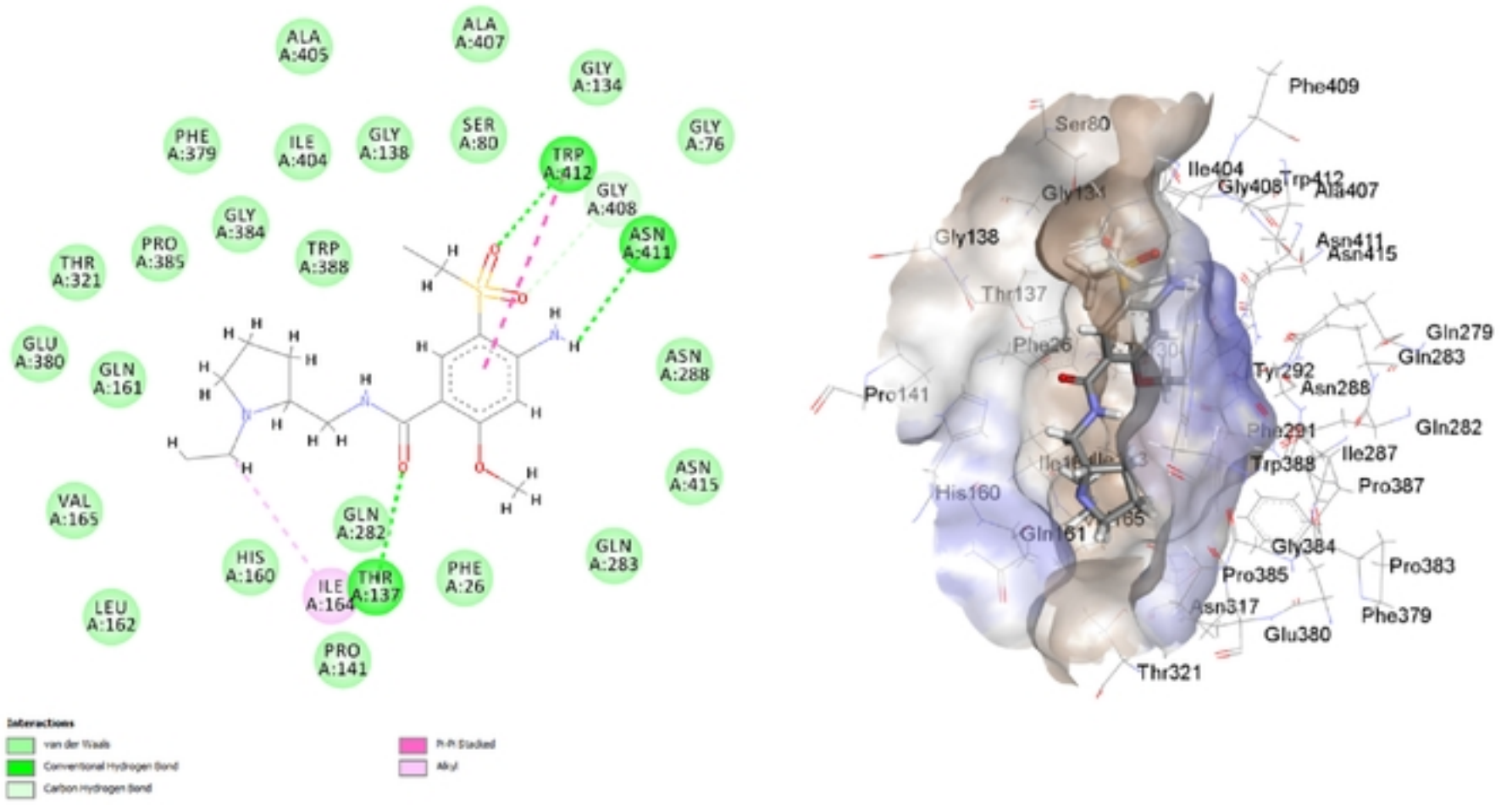
ALA A:405
ALA A:407
GLY A:134
PHE A:379
ILE A:404
GLY A:138
SER A:80
GLY A:76
TRP A:412
GLY A:408
GLY A:384
ASN A:411
THR A:321
PRO A:385
TRP A:388
GLU A:380
GLN A:161
ASN A:288
ASN A:415
VAL A:165
GLN A:282
GLN A:283
HIS A:160
ILE A:164
THR A:137
PHE A:26
LEU A:162
PRO A:141
Interactions
van der Waals
Conventional Hydrogen Bond
Carbon Hydrogen Bond
Pi-Pi Stacked
Alkyl
Phe409
Ser80
Ile404
Gly408
Trp412
Ala407
Gly138
Asn411
Asn415
Thr137
Gln279
Gln283
Tyr292
Asn288
Pro141
Phe291
Gln282
Ile287
Trp388
Pro387
His160
Gln161
Gly384
Pro383
Pro385
Asn317
Phe379
Glu380
Thr321

B:

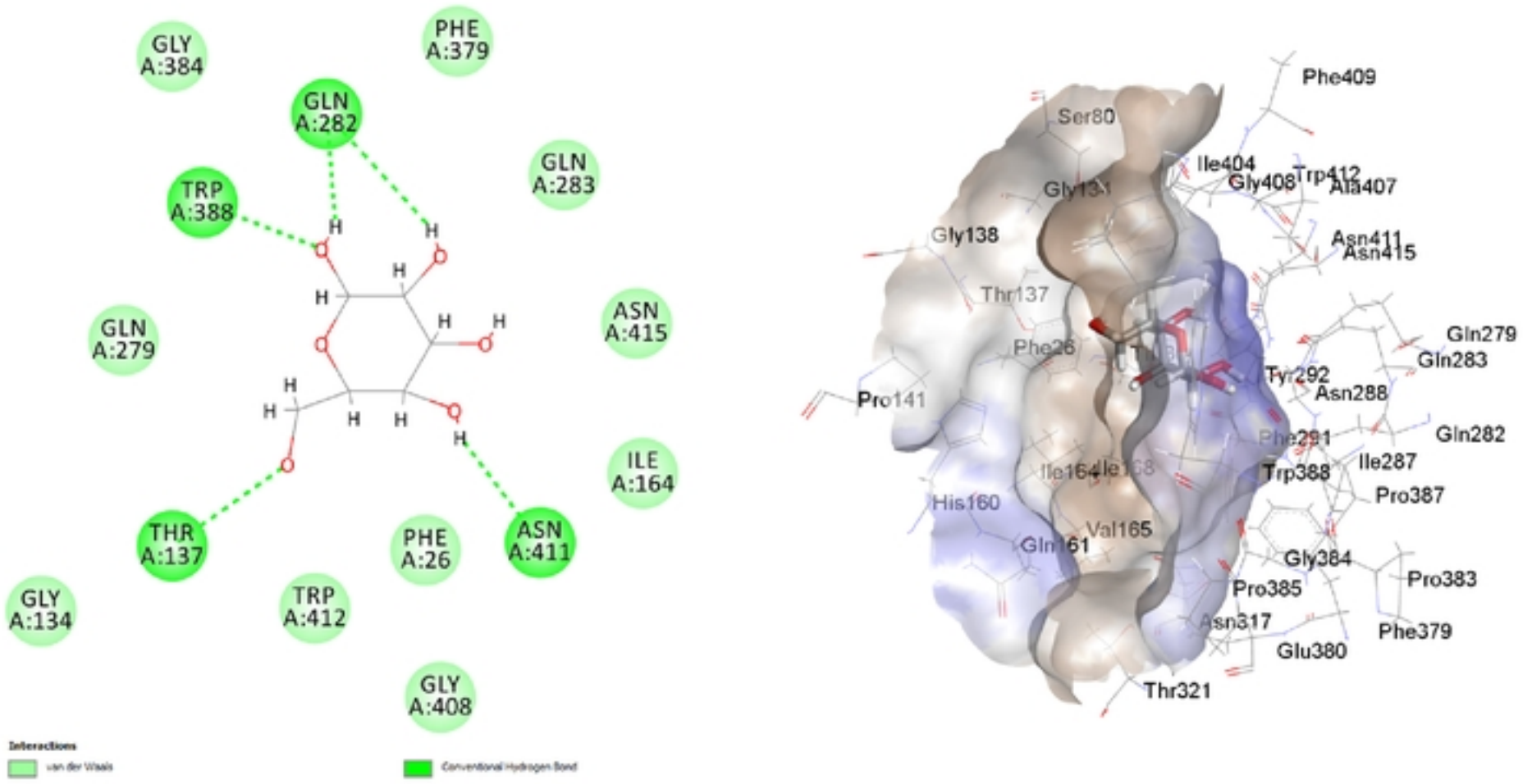
GLY A:384
PHE A:379
GLN A:282
TRP A:388
GLN A:283
GLN A:279
ASN A:415
ILE A:164
THR A:137
PHE A:26
ASN A:411
GLY A:134
TRP A:412
GLY A:408
Interactions
van der Waals
Conventional Hydrogen Bond
Phe409
Ser80
Ile404
Gly408
Trp412
Ala407
Gly138
Asn411
Asn415
Thr137
Gln279
Gln283
Tyr292
Asn288
Pro141
Phe291
Gln282
Ile287
Trp388
Pro387
His160
Val165
Gln161
Gly384
Pro383
Pro385
Asn317
Phe379
Glu380
Thr321

C:

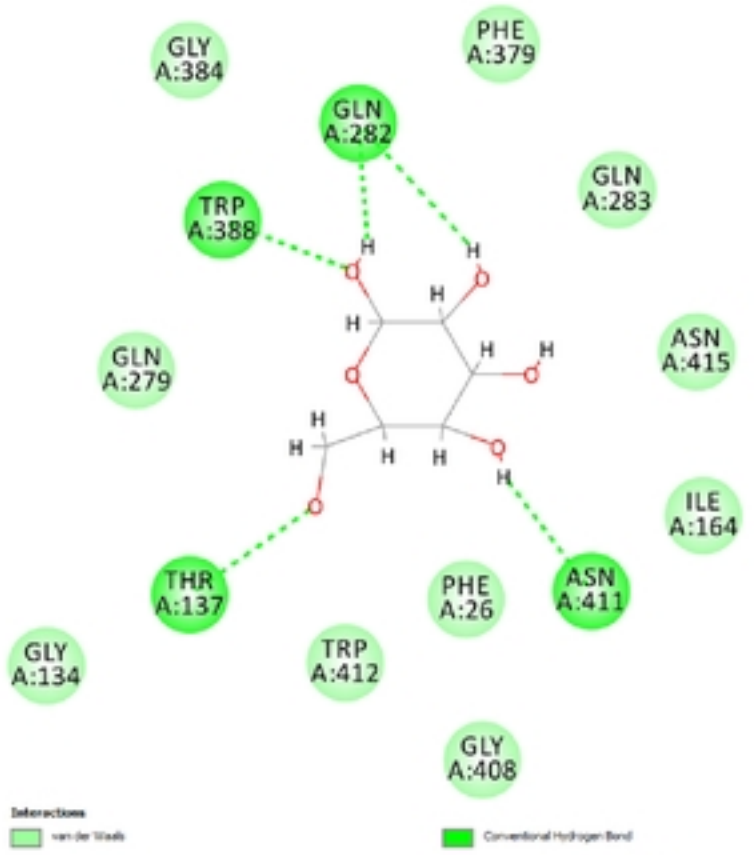
GLY A:384
PHE A:379
GLN A:282
GLN A:283
TRP A:388
GLN A:279
ASN A:415
ILE A:164
THR A:137
PHE A:26
ASN A:411
GLY A:134
TRP A:412
GLY A:408
Interactions
van der Waals
Conventional Hydrogen Bond

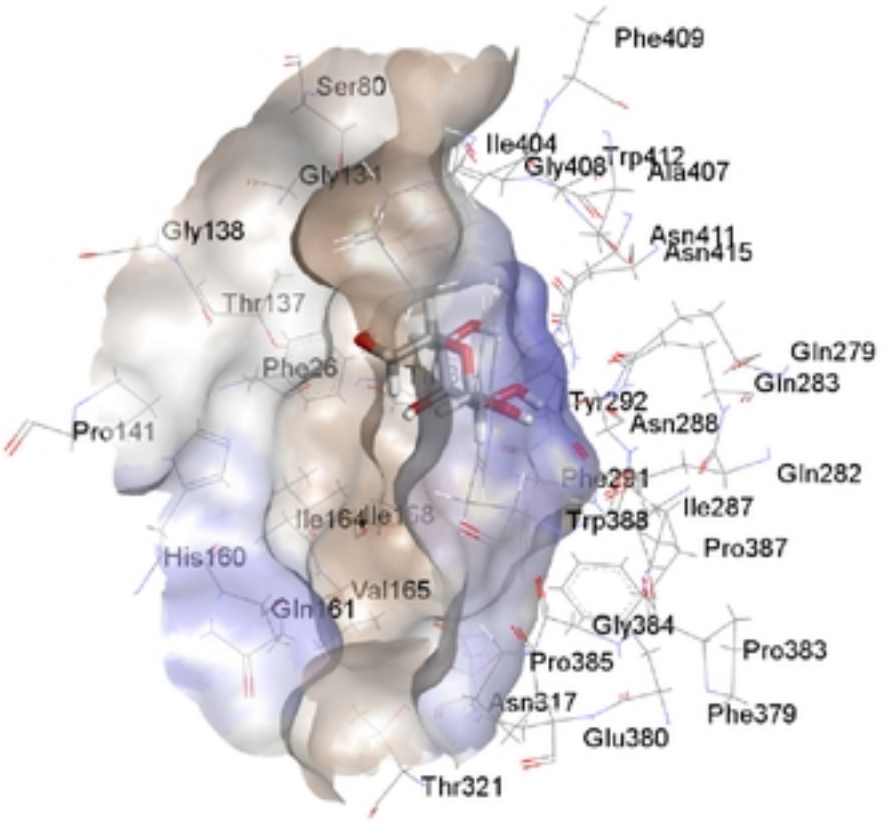
Phe409
Ser80
Ile404
Gly408
Trp412
Ala407
Gly138
Asn411
Asn415
Thr137
Gln279
Gln283
Phe26
Tyr292
Asn288
Pro141
Gln282
Ile287
Trp388
Pro387
His160
Val165
Gly384
Pro383
Pro385
Asn317
Phe379
Glu380
Thr321

D:

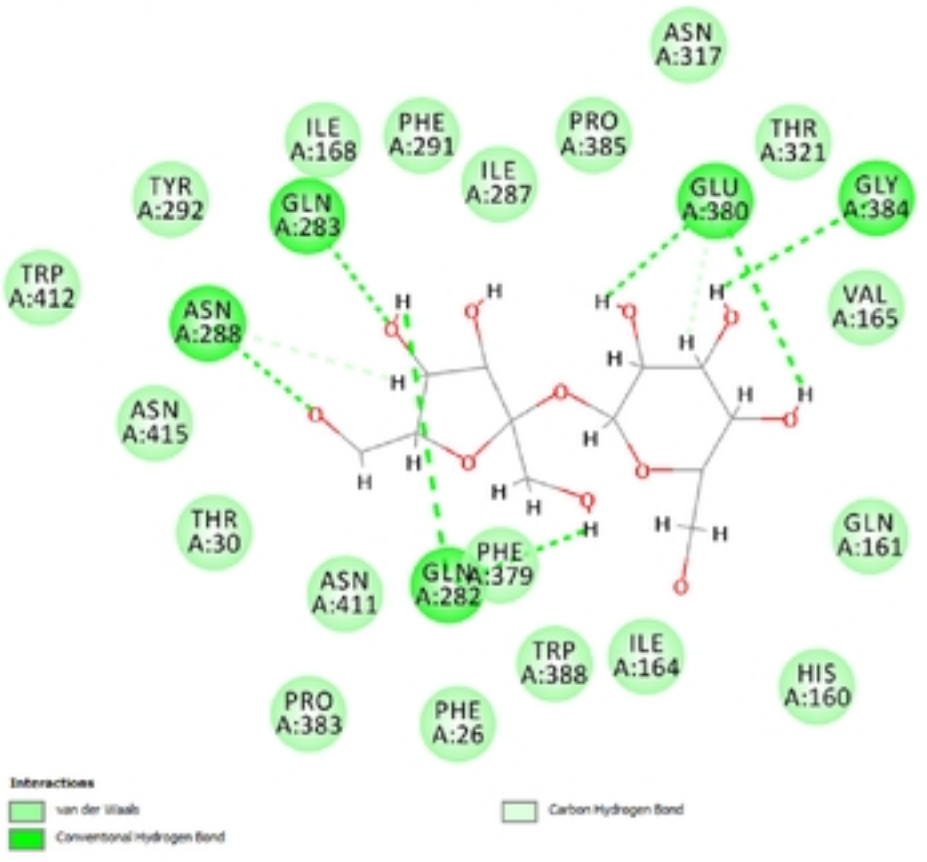
ASN A:317
ILE A:168
PHE A:291
PRO A:385
THR A:321
TYR A:292
GLN A:283
ILE A:287
GLU A:380
GLY A:384
TRP A:412
ASN A:288
VAL A:165
ASN A:415
THR A:30
GLN A:161
ASN A:411
GLN A:282
PHE A:379
TRP A:388
ILE A:164
HIS A:160
PRO A:383
PHE A:26
Interactions
van der Waals
Conventional Hydrogen Bond
Carbon Hydrogen Bond

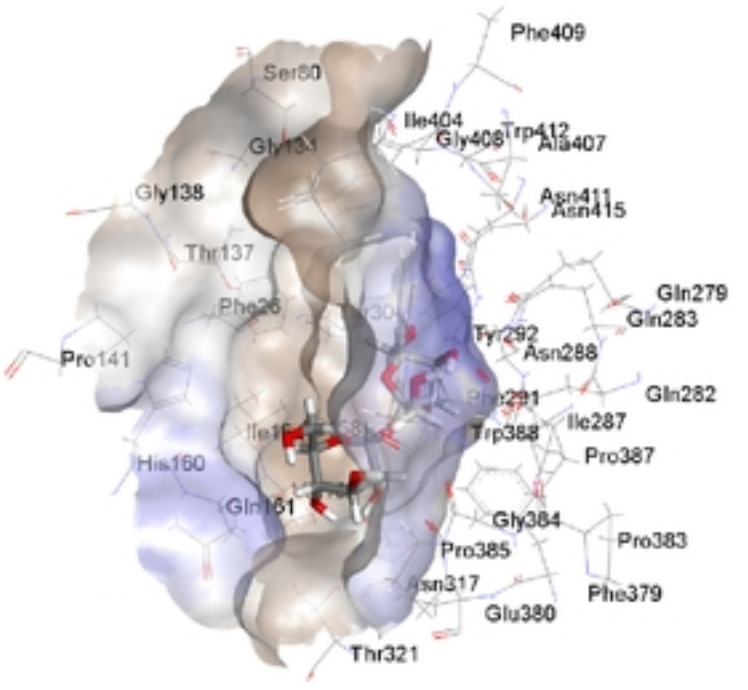
Phe409
Ser80
Ile404
Gly408
Trp412
Ala407
Gly138
Asn411
Asn415
Thr137
Gln279
Gln283
Phe26
Tyr292
Asn288
Pro141
Gln282
Ile287
Trp388
Pro387
His160
Gly384
Pro383
Pro385
Asn317
Phe379
Glu380
Thr321

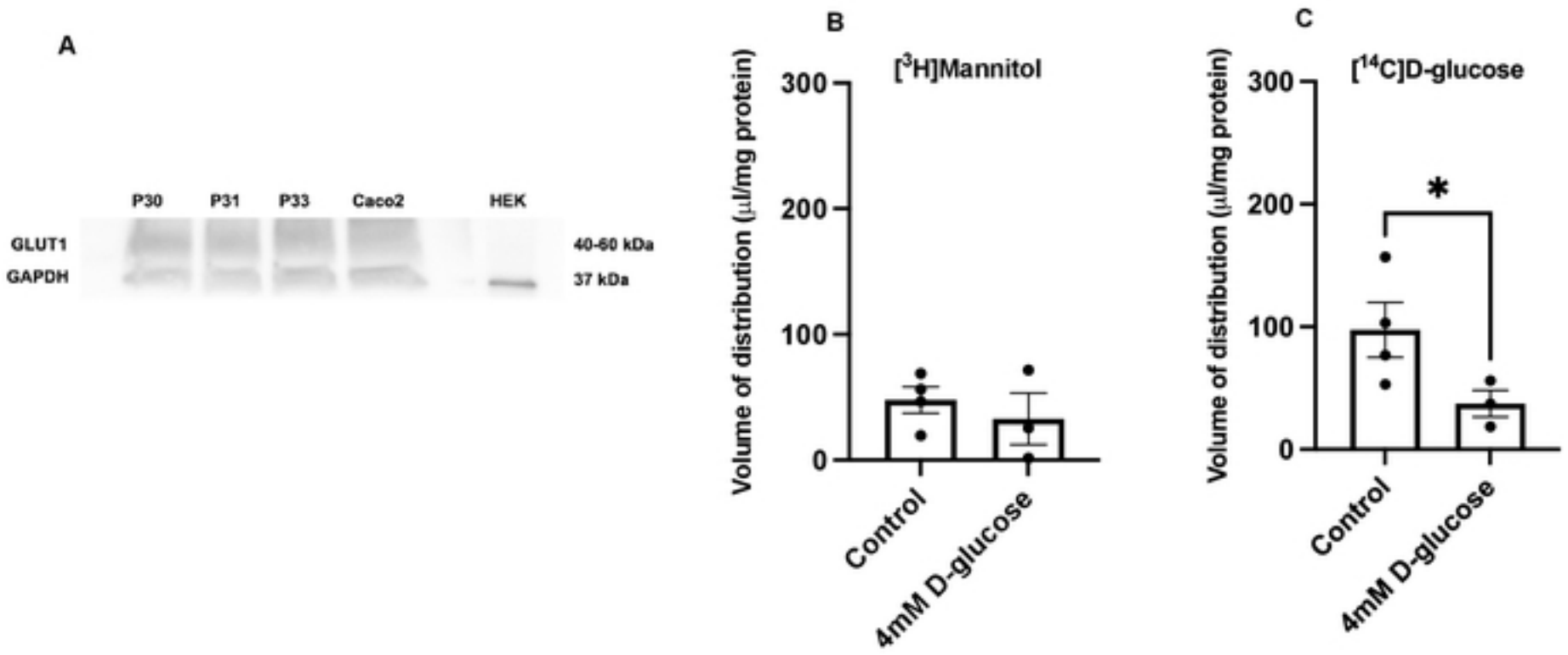
A
P30
P31
P33
Caco2
HEK
GLUT1
GAPDH
40-60 kDa
37 kDa
B
[3H]Mannitol
Volume of distribution (µl/mg protein)
300
200
100
0
Control
4mM D-glucose
C
[14C]D-glucose
Volume of distribution (µl/mg protein)
300
200
100
0
*
Control
4mM D-glucose

Figure 4

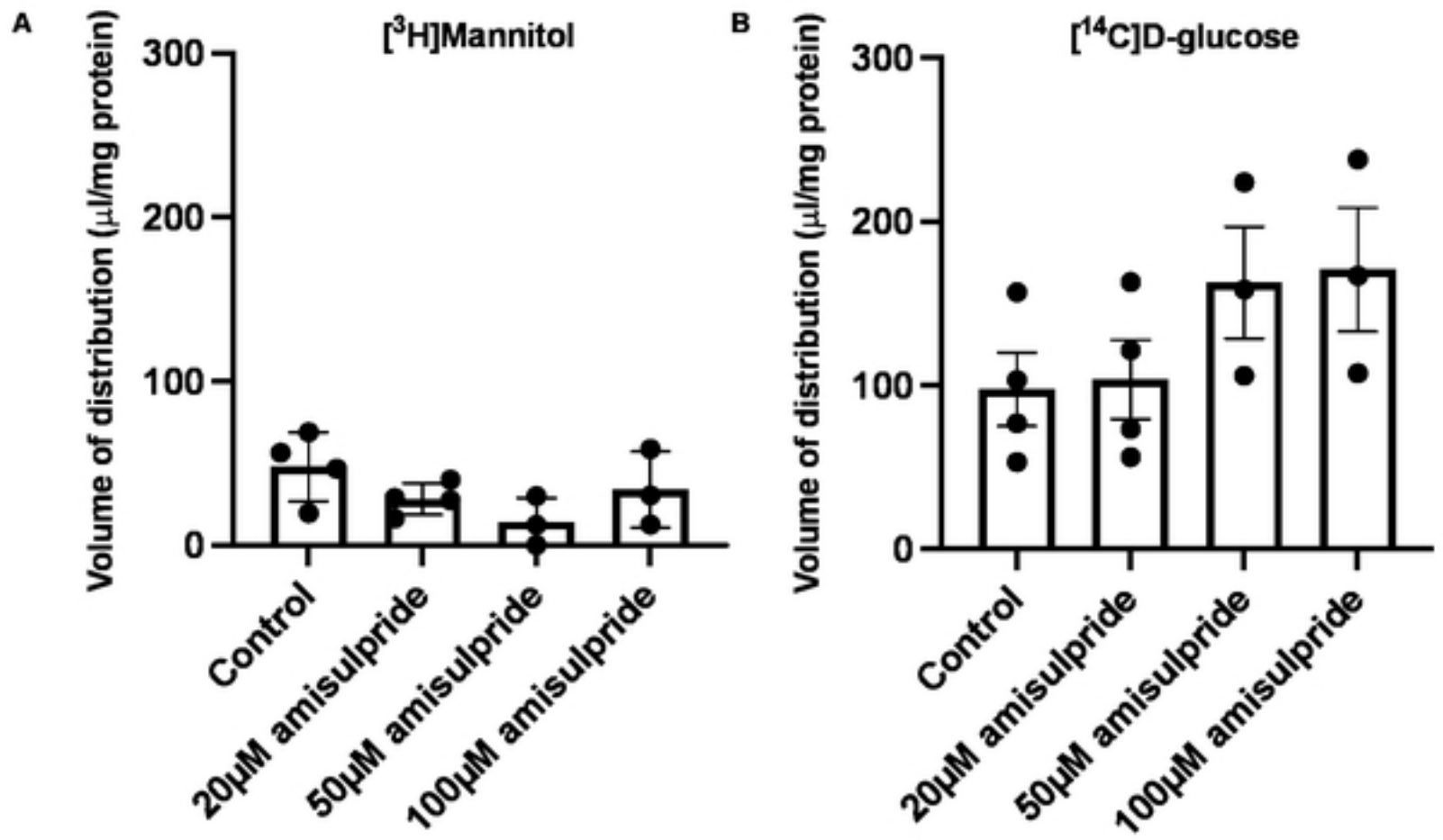
A
[3H]Mannitol
Volume of distribution (µl/mg protein)
300
200
100
0
Control
20µM amisulpride
50µM amisulpride
100µM amisulpride
B
[14C]D-glucose
Volume of distribution (µl/mg protein)
300
200
100
0
Control
20µM amisulpride
50µM amisulpride
100µM amisulpride

Figure 5

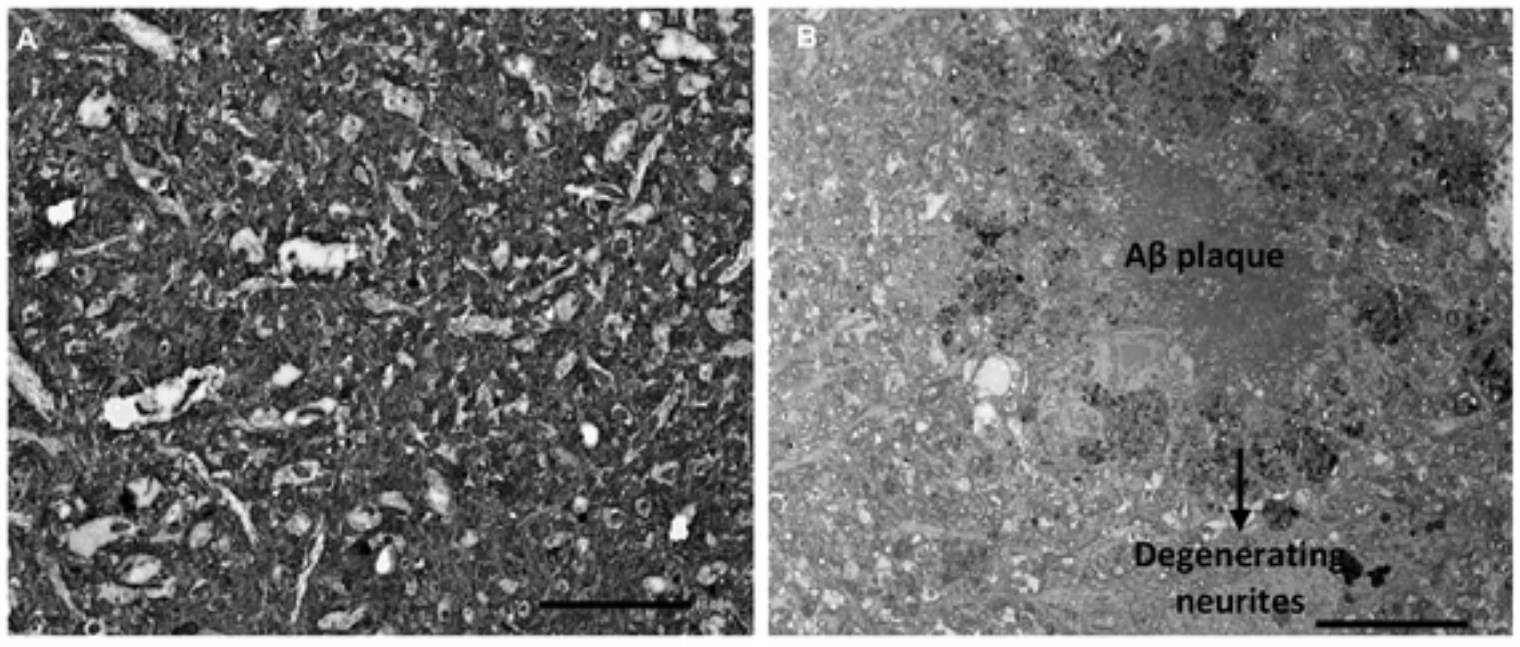

Figure 6

A:

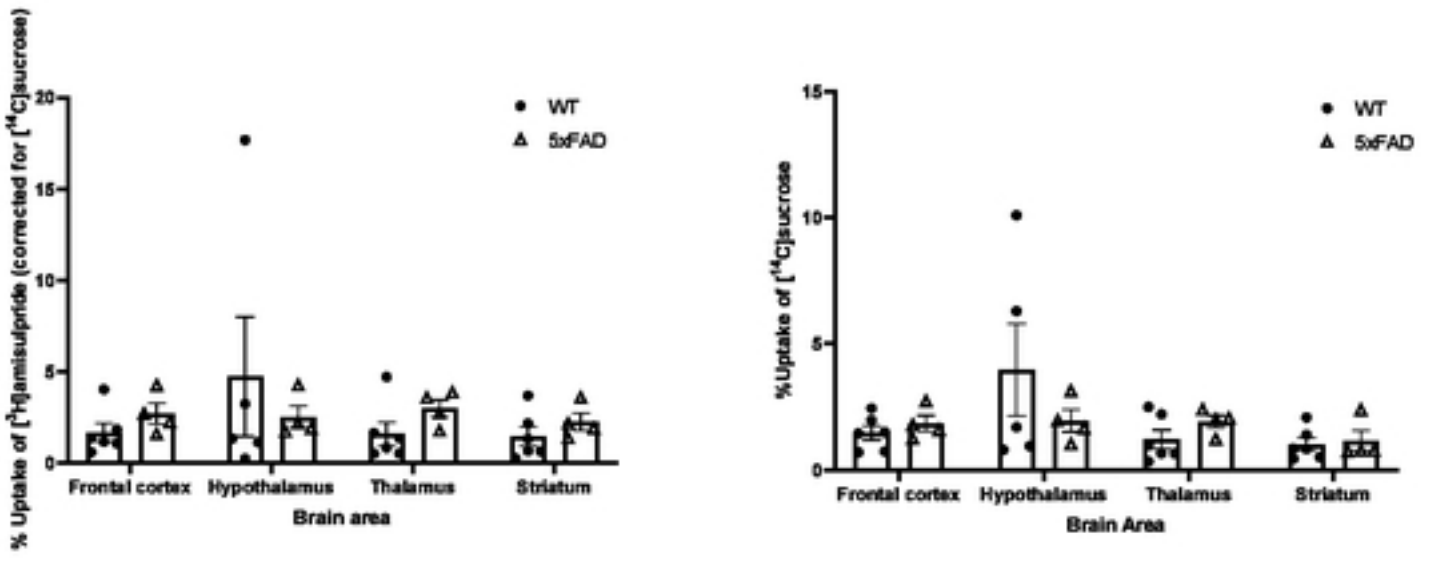
% Uptake of [3H]amisulpride (corrected for [14C]sucrose)
WT
5xFAD
Frontal cortex
Hypothalamus
Thalamus
Striatum
Brain area
%Uptake of [14C]sucrose
Brain Area

B:

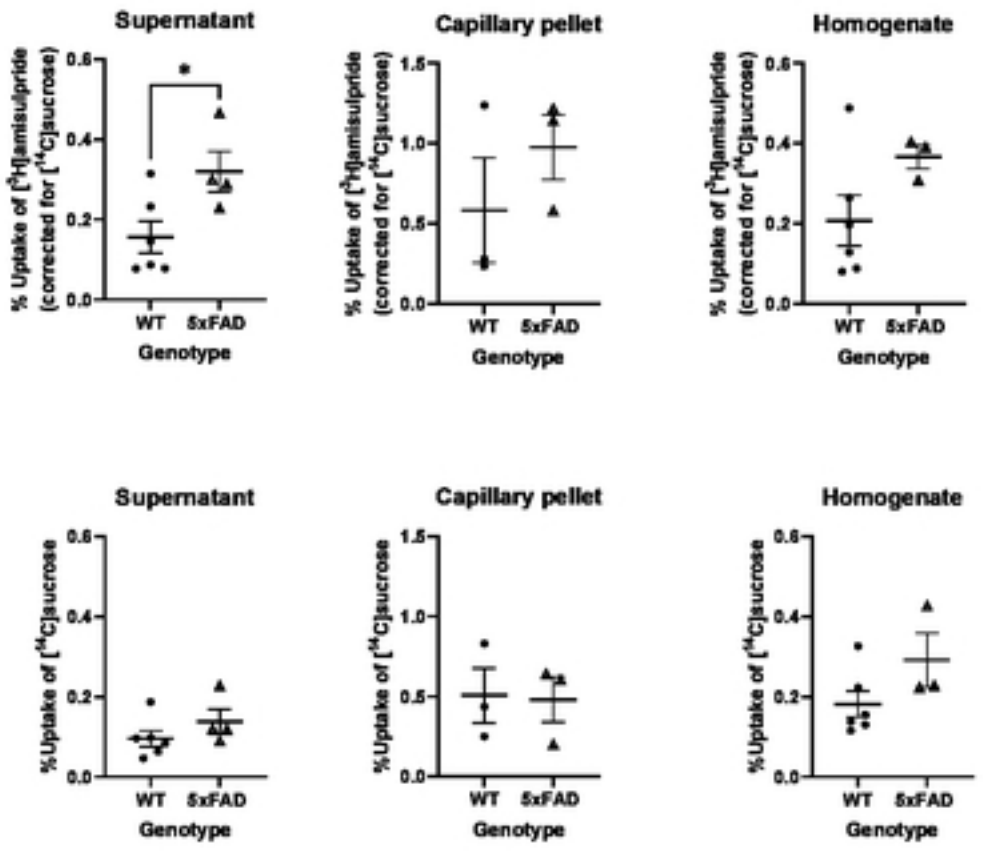
Supernatant
Capillary pellet
Homogenate
% Uptake of [3H]amisulpride (corrected for [14C]sucrose)
%Uptake of [14C]sucrose
WT
5xFAD
Genotype

Figure 7

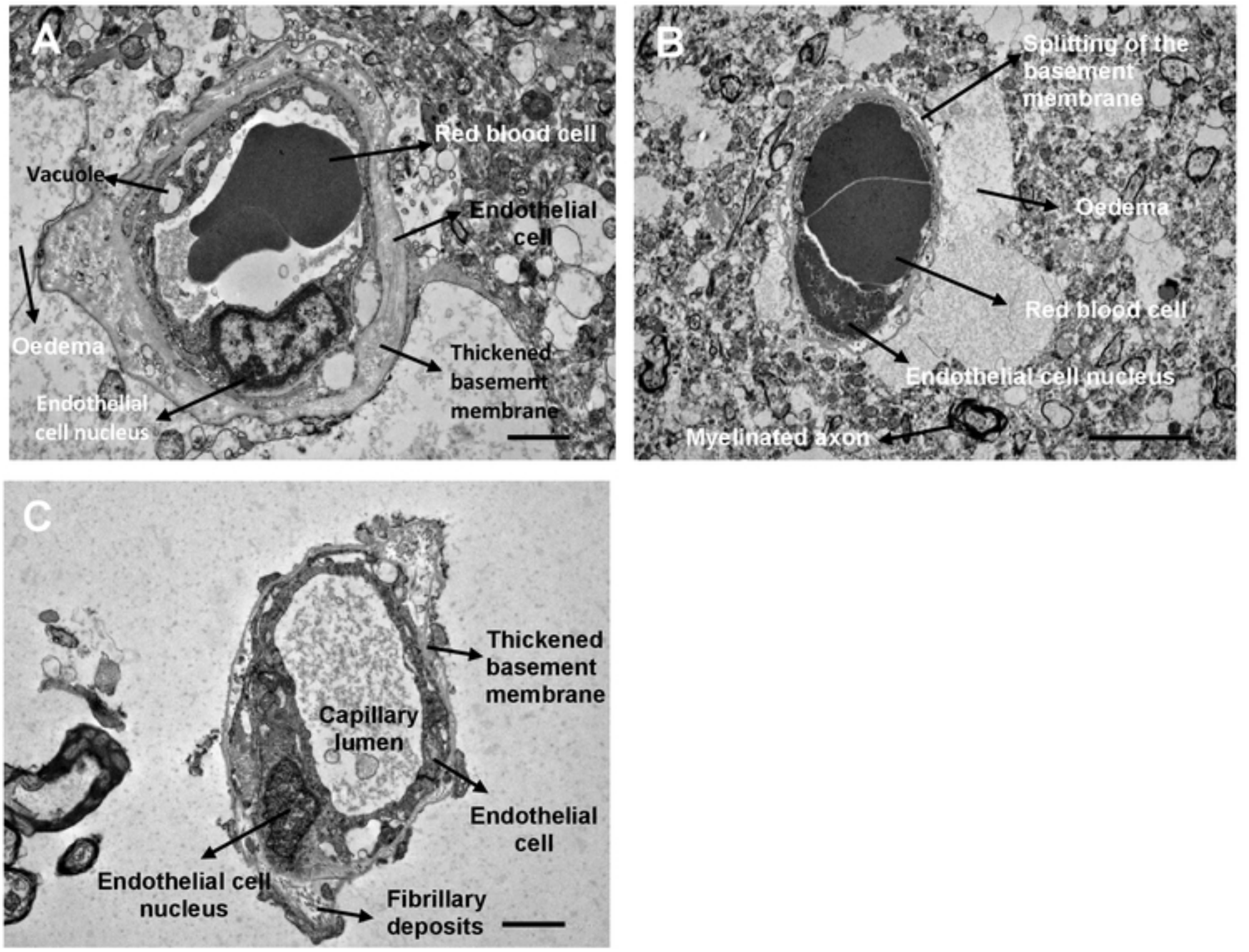
A
Red blood cell
Vacuole
Endothelial cell
Oedema
Thickened basement membrane
Endothelial cell nucleus
B
Splitting of the basement membrane
Oedema
Red blood cell
Endothelial cell nucleus
Myelinated axon
C
Thickened basement membrane
Capillary lumen
Endothelial cell
Endothelial cell nucleus
Fibrillary deposits

Figure 8

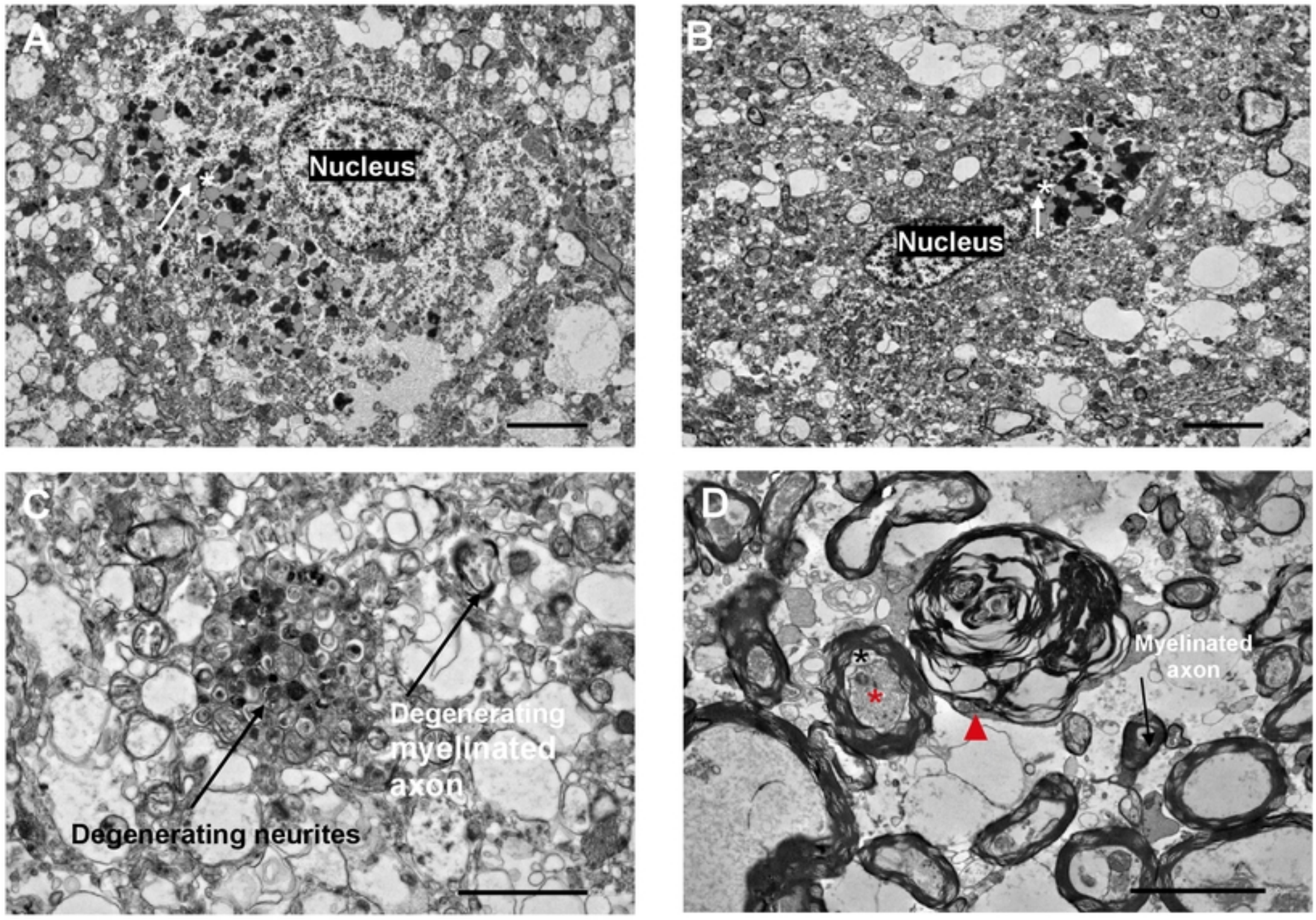

* - electron dense portions of lipofuscin granules, ↗ - lucid portions of lipofuscin granules

* - vacuolisation, ▲ - myelinated whorled masses, * - condensed axonal cytoplasm

Figure 9

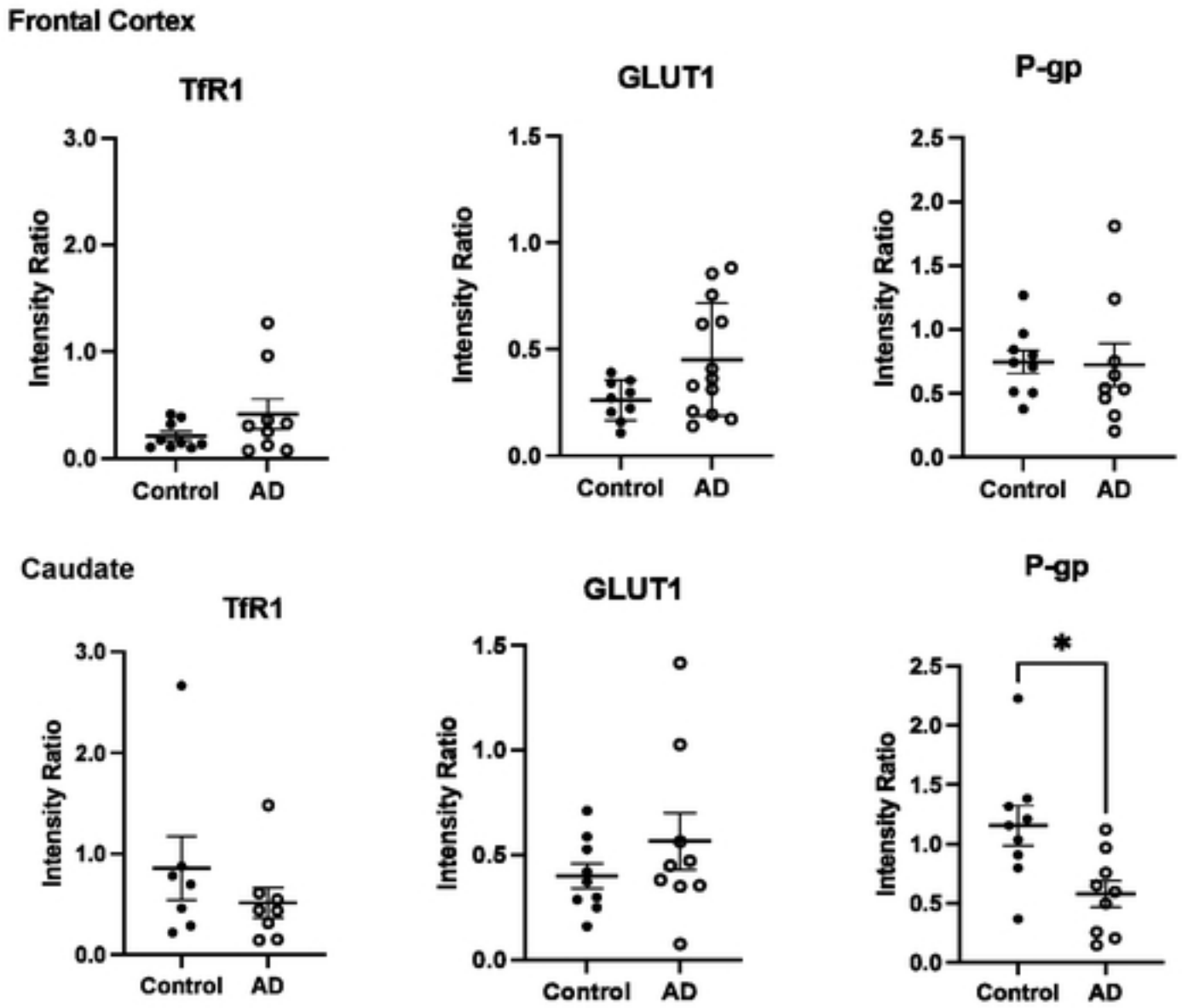
Frontal Cortex
TfR1
GLUT1
P-gp
Intensity Ratio
Control
AD
Caudate
TfR1
GLUT1
P-gp
*

Figure 10

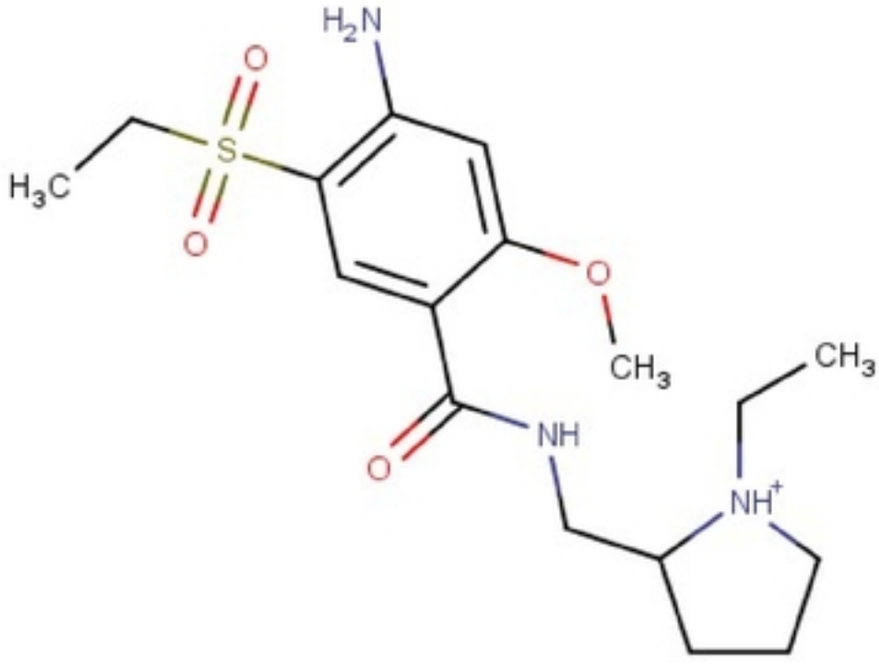

Amisulpride microspecies A (96.77%)

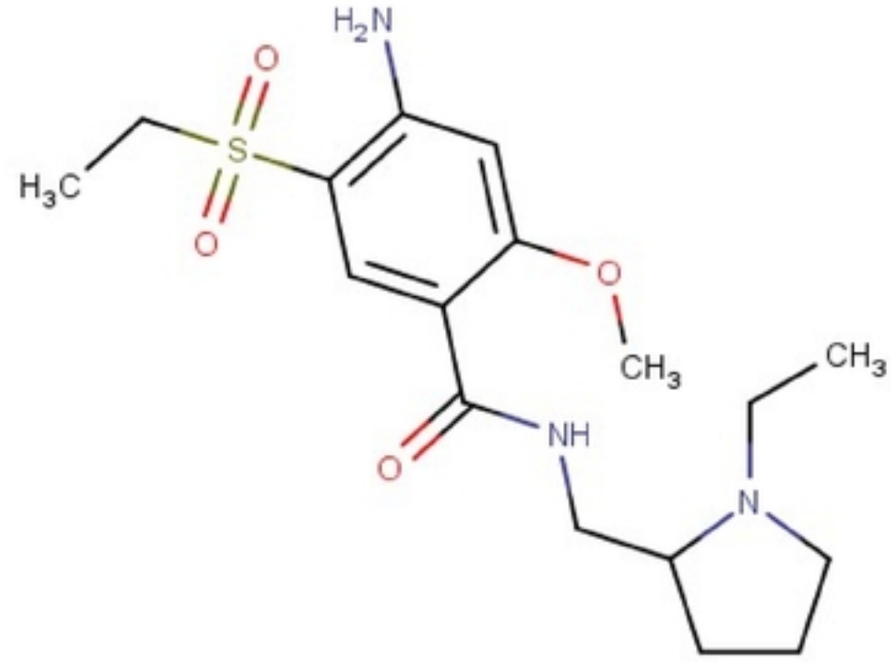

Amisulpride microspecies B (3.23%)

Figure 1